

Modelling of Auxiliary Devices for a Hardware-in-the-Loop Application

Master's thesis
performed at **Vehicular Systems**

by
Johan Olsén

Reg nr: LiTH-ISY-EX-3566-2005

24th February 2005

Modelling of Auxiliary Devices for a Hardware-in-the-Loop Application

Master's thesis

performed at **Vehicular Systems,**
Dept. of Electrical Engineering
at **Linköpings universitet**

by **Johan Olsén**

Reg nr: LiTH-ISY-EX-3566-2005

Supervisor: **Johan Jonsson**
DaimlerChrysler AG
Anders Fröberg
Linköpings universitet

Examiner: **Associate Professor Lars Eriksson**
Linköpings universitet

Linköping, 24th February 2005

	Avdelning, Institution Division, Department Vehicular Systems, Dept. of Electrical Engineering 581 83 Linköping	Datum Date 24th February 2005
	Språk Language <input type="checkbox"/> Svenska/Swedish <input checked="" type="checkbox"/> Engelska/English <input type="checkbox"/> _____	Rapporttyp Report category <input type="checkbox"/> Licentiatavhandling <input checked="" type="checkbox"/> Examensarbete <input type="checkbox"/> C-uppsats <input type="checkbox"/> D-uppsats <input type="checkbox"/> Övrig rapport <input type="checkbox"/> _____
URL för elektronisk version http://www.vehicular.isy.liu.se http://www.ep.liu.se/exjobb/isy/2005/3566/		
Titel	Modellering av hjälppaggregat för en hardware-in-the-loop-applikation	
Tide	Modelling of Auxiliary Devices for a Hardware-in-the-Loop Application	
Författare Author	Johan Olsén	
Sammanfattning Abstract	<p>The engine torque is an important control signal. This signal is disturbed by the devices mounted on the belt. To better be able to estimate the torque signal, this work aims to model the auxiliary devices' influence on the crankshaft torque. Physical models have been developed for the air conditioning compressor, the alternator and the power steering pump. If these models are to be used in control unit function development and testing, they have to be fast enough to run on a hardware-in-the-loop simulator in real time. The models have been simplified to meet these demands.</p> <p>The compressor model has a good physical basis, but the validity of the control mechanism is uncertain. The alternator model has been tested against a real electronic control unit in a hardware-in-the-loop simulator, and tests show good results. Validation against measurements is however necessary to confirm the results. The power steering pump model also has a good physical basis, but it is argued that a simple model relating the macro input-output power could be more valuable for control unit function development.</p>	
Nyckelord Keywords	Auxiliary Devices, Air Conditioning Compressor, Alternator, Power Steering Pump, Hardware-in-the-Loop	

Abstract

The engine torque is an important control signal. This signal is disturbed by the devices mounted on the belt. To better be able to estimate the torque signal, this work aims to model the auxiliary devices' influence on the crankshaft torque. Physical models have been developed for the air conditioning compressor, the alternator and the power steering pump. If these models are to be used in control unit function development and testing, they have to be fast enough to run on a hardware-in-the-loop simulator in real time. The models have been simplified to meet these demands.

The compressor model has a good physical basis, but the validity of the control mechanism is uncertain. The alternator model has been tested against a real electronic control unit in a hardware-in-the-loop simulator, and tests show good results. Validation against measurements is however necessary to confirm the results. The power steering pump model also has a good physical basis, but it is argued that a simple model relating the macro input-output power could be more valuable for control unit function development.

Keywords: Auxiliary Devices, Air Conditioning Compressor, Alternator, Power Steering Pump, Hardware-in-the-Loop

Preface

This thesis concludes my studies at the M.Sc. programme in Applied Physics and Electrical Engineering. The main work was carried out at the DaimlerChrysler department for powertrain control, REI/EP, in Esslingen am Neckar, Germany between February and October 2004. This final report was written at the library at Chalmers School of Technology, Gothenburg, Sweden, during the following winter months.

Acknowledgment

First of all I would like to thank my supervisor Johan Jonsson at DaimlerChrysler who always listened carefully and came with good suggestions to whatever problem I had. At DaimlerChrysler I would also like to thank Thorsten Engelhardt and Magnus Ramstedt for their insight and support during HiL simulations, Christian Kringe for providing me with his battery model and project leader Zandra Jansson for her feedback and support.

I would also like to thank my co-supervisor Anders Fröberg at Linköpings universitet for pointing out directions for this thesis. Furthermore, literature provided by Marcus Rösth, Linköpings universitet and Gary DesGroseilliers, Massachusetts Institute of Technology was very helpful and their help should not go unmentioned.

Contents

Abstract	v
Preface and Acknowledgement	vi
1 Introduction	1
1.1 Thesis Outline	2
2 Auxiliary Devices Theory	4
2.1 Air Conditioning Compressor	4
2.1.1 Refrigerant Circuit	4
2.1.2 Swash Plate Compressor	5
2.1.3 Refrigerant	7
2.2 Alternator	8
2.2.1 Electrodynamics	8
2.2.2 Three-Phase Power	10
2.2.3 Rectification	11
2.2.4 Excitation Circuit and Control	12
2.3 Power Steering Pump	13
2.3.1 Servo System	13
2.3.2 Power Steering Pump	14
3 Modelling Theory	16
3.1 Complexity	16
3.2 Method	17
3.3 Stability	18
3.4 Validation	19
4 Modelling	20
4.1 AC Compressor	21
4.1.1 Piston Kinematics	21
4.1.2 Adiabatic Process	23
4.1.3 The Compression Cycle	25
4.1.4 Deduction of Torque	25

4.1.5	Mass Flow and Control	26
4.2	Alternator	27
4.2.1	Rotor	28
4.2.2	Magnetic Field	29
4.2.3	Armature Windings	30
4.2.4	Torque	33
4.3	Power Steering Pump	33
4.3.1	Simple Model	33
4.3.2	Vane Dynamics	34
4.3.3	Hydraulic Seal	37
4.3.4	Fluid Dynamics	37
4.3.5	Torque	39
5	HiL and Real Time Adaptation	41
5.1	Hardware-in-the-Loop	41
5.2	Real Time Adaptation	42
5.2.1	AC Compressor	43
5.2.2	Alternator	43
5.2.3	Power Steering Pump	45
6	Simulations and Validation	46
6.1	High Resolution MiL Simulations	46
6.1.1	AC Compressor	46
6.1.2	Alternator	47
6.1.3	Power Steering Pump	49
6.2	HiL Simulation	50
6.3	Validity Discussion	51
7	Conclusions	53
8	Further Work	55
	References	57
	Notation	59

Chapter 1

Introduction

Vehicles of today are heavily dependent on electronics. Their design is evolving into the co-design of mechanics and control [1]. Modern vehicles are equipped with Electronic Control Units (ECUs), which controls various functions of the vehicle. Possibilities to control vehicle parts to work in unison can make them more efficient, which leads to lower fuel consumption.

The engine torque is one of the vehicle's most important control signals. This is the torque of the crankshaft, which is transferred out to the drive line and in the end, the wheels. However, an engine has more functions than just rotating the wheels and propelling the vehicle. It is also responsible for delivering power to other systems in the vehicle. These are the air conditioning system, the electric system, the power steering system and some more. The chief sources of power for these systems are the auxiliary devices, which are the air conditioning compressor, the alternator and the power steering pump. They are driven by a belt mounted over the crankshaft gear. To the crankshaft they act as loads, disturbing the torque going out to the drive line.

Naturally, the magnitude of the individual torques taken by the auxiliary devices varies in different situations. The physical characteristics of the devices can explain and foresee these variations. Mathematical models, based on the laws of physics can thus be used to simulate how large the individual torques are in different situations. These models can then be used to better simulate the characteristics of the engine torque.

When firmware to a new ECU is constructed, a vehicle to test and evaluate it on during development is almost a necessity. However, building test vehicles is very expensive, especially when several models and configurations are to be considered. A much more suitable alternative is to use modelling and simulation for development and product testing. To run real hardware against a modelled system, testing in a Hardware-in-the-Loop (HiL) system is very

useful.

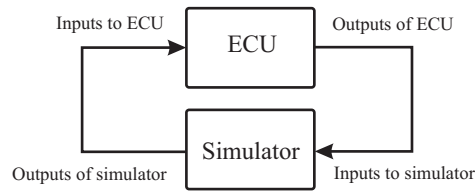


Figure 1.1: The Hardware-in-the-Loop system

A HiL simulator is a type of embedded system whose main functionality can be described by Figure 1.1.

Software models of the systems controlled by, and influencing, the ECU can be implemented in the HiL simulator. Some of these systems are the auxiliary devices. Demands on the HiL simulation models will be that they behave like the real systems and that they are able to run in real-time. During a simulation the models will have to respond to the ECU's control signals, like they would have in a real-world testing situation.

The main objective of this work is to develop models of the auxiliary devices and implement them in a real-time HiL simulator. These models are to be based on the laws of physics. Throughout the thesis various modelling techniques will be presented and used to model the air conditioning compressor, the alternator and the power steering pump. The models' behavior will then be evaluated. A brief presentation of the various chapters is given below.

1.1 Thesis Outline

Chapter 1 - Introduction

Chapter 2 - Auxiliary Devices Theory The air conditioning compressor, the alternator and the power steering pump are introduced. Their structure, configuration and functionality is briefly presented.

Chapter 3 - Modelling Theory A short discussion about model complexity, modelling methods and a background to later modelling is presented.

Chapter 4 - Modelling Models for the air conditioning compressor, the alternator and the power steering pump are constructed and presented.

Chapter 5 - HiL and Real Time Adaptation The simplifications and adjustments to the models in order to achieve HiL testability and an executable system are being presented here.

Chapter 6 - Simulations and Validation The results of the simulations are presented. The models' reliability are examined.

Chapter 7 - Conclusions

Chapter 8 - Further Work

Chapter 2

Auxiliary Devices Theory

On a regular engine a belt is mounted on the crankshaft gear. This belt drives a number of devices, of which this thesis will focus on the air conditioning compressor, the alternator and the power steering pump. There are other auxiliary devices (e.g. the water pump), that have lower energy consumption, and thereby affect the engine torque less. Therefore, they will not be covered by this thesis. In this chapter the structure, configuration and functionality of the three chosen devices will be presented.

2.1 Air Conditioning Compressor

The basic principle that makes an air conditioning (AC) system work is that a liquid going into a gaseous state absorbs heat from its surroundings.

2.1.1 Refrigerant Circuit

The system uses a refrigerant going through different phases in a closed circuit to achieve its purpose. The main components of the system are:

- Compressor
- Condenser
- Evaporator

In the evaporator the low pressure liquid refrigerant is vaporized to gaseous state. The evaporator is a long tube, going back and forth in front of the fan blowing air into the interior of the vehicle. The hot outside air causes the refrigerant going through the evaporator to boil. Heat from the air is hereby absorbed by the refrigerant, cooling the air which blows into the coupé. From the evaporator the gas flows to the compressor where it is compressed. Both

pressure and temperature of the refrigerant are hereby highly heightened. Next, the gas flows to the condenser, which similarly to the evaporator is a long tube going back and forth. Here, the heat transfer takes place from the refrigerant to the surrounding air, resulting in a change from gaseous to liquid state. The refrigerant is cooler but its high pressure is maintained as it flows back to the evaporator, via an expansion valve, thus closing the circuit. The expansion valve maintains the pressure difference between condenser output flow and evaporator input flow.

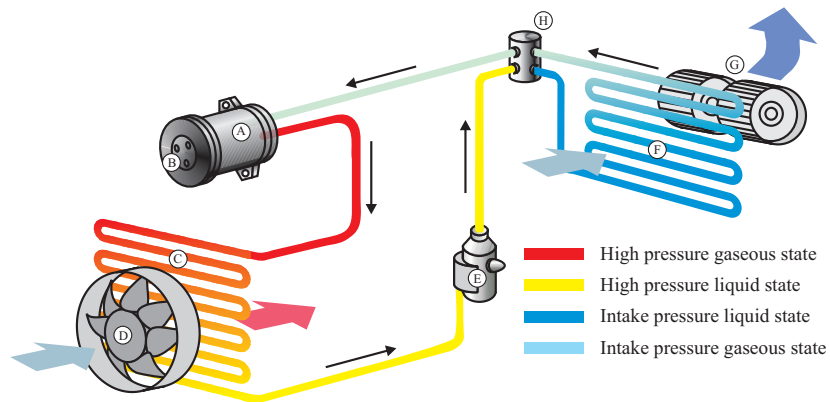


Figure 2.1: Refrigerant circuit, with components: A) Compressor, B) Compressor clutch, C) Condenser, D) Condenser fan, E) High-pressure relief valve, F) Evaporator, G) Ventilation fan and H) Expansion valve

There are more components in the refrigerant circuit, but they have little to do with the main cooling functionality. The cooling capacity of the system is determined by the flow of refrigerant through the circuit. Figure 2.1 shows the refrigerant circuit.

2.1.2 Swash Plate Compressor

The most common compressor types in the automotive industry are reciprocating compressors and among these the most common is the swash plate compressor [2]. It compresses the refrigerant using a piston and cylinder system.

The compressor has a rotating pulley on one side. The belt is mounted over this pulley, rotating it with a speed proportional to the crankshaft rotation. This rotating motion is converted to reciprocating motion by the *swash plate*, a tilted disc mounted on the rotating axle. The reciprocating motion is par-

allel to the centerline of the rotating shaft. During rotation, positions on the disc will alternate between different axial positions. One revolution of the pulley and disc will translate to one period, where pistons mounted in contact with the disc (via a ball-and-socket joint and a slipper) go from maximum to minimum displacement and back again. A sketch of a typical swash plate compressor can be seen in Figure 2.2.

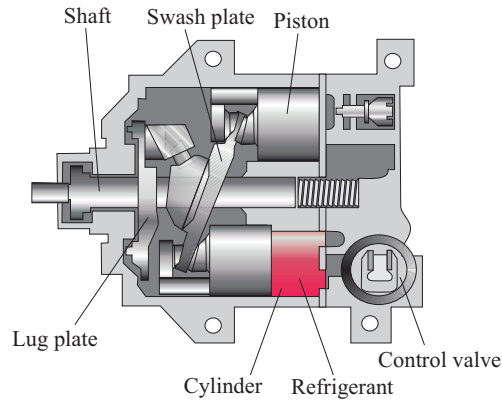


Figure 2.2: The swash plate compressor

The pistons compress the refrigerant and thereby pump it around the closed circuit. Due to the piston system, one can speak of a stroke cycle. There are two piston strokes for each cycle. This cycle contains an intake stroke (suction), a compression and a discharge of the high-pressurized refrigerant. During suction, the refrigerant pressure inside the cylinder will be constant, the *intake pressure*. The *discharge pressure* is decided by the pressure-relief valves, which are situated in one end of the cylinder. There are numerous structures for such valves, but they all function similarly. The simplest form is probably the *spring-loaded ball valve* depicted in Figure 2.3. The pressure in the cylinder acts on one side of the ball, while a spring provides a mechanical load on the other side. When the cylinder pressure force overcomes the

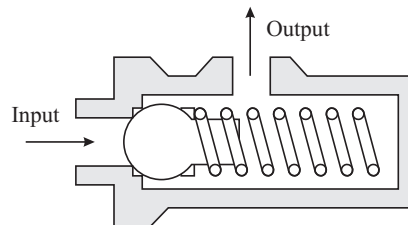


Figure 2.3: Pressure control valve

spring force, causing the valve to open, the high pressure refrigerant will flow through the valve. These types of valves often have tendency to chatter [3].

To make the refrigerant flow delivered by the compressor, and thereby also the cooling capacity, invariable of the rotational speed, modern systems use a swash plate with variable tilt angle. The angle of the swash plate can be controlled in different ways. It can be internally regulated, which means that an integrated regulating valve keeps the pressure in the crankcase constant. Refrigerant flows via this valve between the cylinders. When the swash plate angle is externally regulated, a signal controls the definite angle to the cranking axle. This makes it possible to change the cylinder stroke volume and thereby the flow of refrigerant. It is usually good to be able to switch between internal and external regulation. Transient pulses on the crank, such as large motor speed increases, could otherwise damage the compressor.

The number of cylinders in a swash plate compressor can vary, usually between 2 and 7, mounted circularly in parallel with the rotating axle.

2.1.3 Refrigerant

The refrigerant's aggregated state changes constantly between gas and liquid. A greasing oil is mixed with the refrigerant to hinder friction and wear on the mechanical parts of the cooling system.

CFCs (Chlorofluorocarbons) and especially Freon were commonly used in old refrigerant systems. It was considered a good refrigerant because of good thermal capacities and its unreactivity. However, its unreactivity also makes it one of the worst pollutants, contributing heavily to ozone depletion and the greenhouse effect [4].

Today, regulations enforce the use of less environmentally damaging refrigerants, and the industry standard is the HFC (hydrofluorocarbon) R-134a with the chemical formula CH_2FCF_3 . Proposed new regulations to limit the use of fluor gases can prohibit this substance after year 2010 [5]. Alternatives, like propane, are environmentally friendlier but have less cooling capability (and can thereby affect the global warming as much as R-134a, due to the higher fuel consumption for a less effective cooling system [6]). In this work, R-134a will be assumed legal and therefore the models will be based on that refrigerant.

The thermodynamic and fluid properties of a refrigerant determine how easily it can flow through the compressor. The pressure-volume characteristics are usually described in a p-V diagram. Such diagrams are available for different refrigerants in most good textbooks on applied thermodynamics, for example [7].

2.2 Alternator

The vehicle's electrical system gets its power from two sources: the battery and the alternator (AC generator). The battery is used as an energy reservoir, delivering electricity in situations where the alternator is unable to, for example during engine standstill. The operating alternator delivers current to the battery if it needs charging. A schematic of the electrical system is seen in Figure 2.4

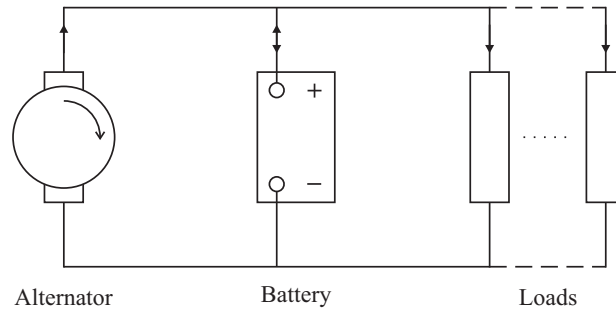


Figure 2.4: The automotive electrical system

2.2.1 Electrodynamics

In generators, magnetic fields are used for converting between different energy forms. Electricity is generated through the principle of *electromagnetic induction*. A current flowing through a wire produces a magnetic field around it. When an electric conductor cuts through (moves perpendicular to) a magnetic field, a voltage is induced in it. The opposite, when the field lines of a moving magnetic field cut through a conductor's path, gives the same results.

The *rotor* is the rotating structure of the generator, it has north and south magnetic poles from which a magnetic field originates. The polarity is usually produced by a rotor winding, a wire conductor around an iron core. When a current flows through this wire the magnetic field is produced. The *stator* is usually placed around the rotor, and has a number of windings symmetrically distributed, see Figure 2.5.

When the rotor's magnetic field lines cut through a stator winding, a voltage is induced. This voltage produces currents in the stator winding, thus the conversion from mechanical to electrical energy is completed. However, the induced currents flowing through the stator windings also produce magnetic fields and just as a compass needle tries to align with Earth's magnetic field,

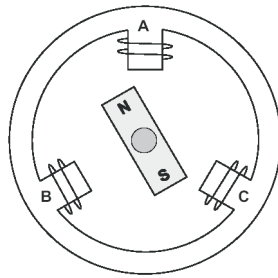


Figure 2.5: Salient pole rotor and three stators

these two sets of fields attempt to align. Torque on the rotor can be associated with their displacement [8]. Energy losses in the generator can be associated with magnetic field leakage, the non-linear magnetization and demagnetization of the rotor core (hysteresis) and eddy current losses. The last two are heat losses and cause heating of the rotor core [9].

An alternator is a vehicular generator that produces alternating currents. The most common alternator type used in the vehicle industry is the *claw pole* (Lundell) alternator. Its rotor consists of two circular bodies of different polarity, with "claws" protruding against the other body. Between the two, the excitation wire is wound. A sketch of the claw pole rotor can be seen in Figure 2.6.

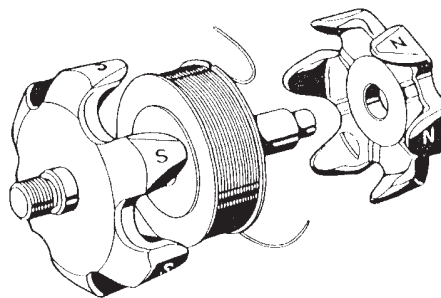


Figure 2.6: Claw pole principle [10]

The magnetic fields will be somewhat asymmetric, but the field lines will enter the metal rotor perpendicularly through the south pole claws, and exit perpendicularly through the north pole claws. Within the rotor the field has been amplified by the encircling excitation winding. In the air gap between rotor and stator, it is therefore believable that the field is reasonably radially

oriented. On the stator side of the system the field lines first go through a laminated iron frame and then bend circularly 180° to go back through the iron frame, over the air gap and back into the south rotor pole. The stator windings are cut by the field lines on the stator side of the iron frame. On the stator side, the field paths in a salient pole alternator and in a claw pole alternator are equal.

2.2.2 Three-Phase Power

Three-phase power uses three alternating electric voltages, stemming from three different stator windings. The voltages are sinusoidal functions of time, all with the same frequency, but with differing phases. The phase separation is 120° or $\frac{2\pi}{3}$ radians.

Normally, this set-up would require six connections for the stator windings. However, by interconnecting the windings with each other, voltage or current gains are possible. There are two types of connections used in three phase systems, the Δ -connection and the Y-connection (often called the star connection). Most alternators use the Y-connection which is depicted in Figure 2.7.

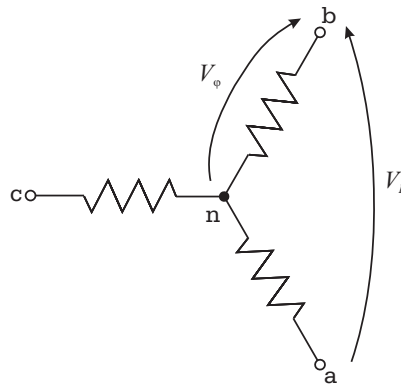


Figure 2.7: 3-Phase Y-connection

By connecting all the stator return wires to the same point n , called the neutral, the same current as if they were not connected will flow through each winding. Moreover, the line voltage V_L between ends will be higher than the individual winding voltage V_ϕ , thanks to the phase differences. The line voltage is $V_L = \sqrt{3}V_\phi$ [11].

2.2.3 Rectification

The battery and the rest of the electrical system require DC output power, and the alternator produces AC power. To transform between the two systems, a diode rectification bridge is used. The three-phase system would need three pairs of power diodes in a set up like in Figure 2.8.

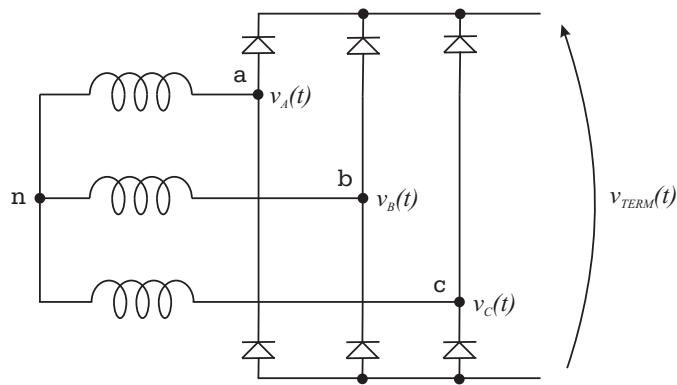


Figure 2.8: 3-Phase rectifier bridge

The rectification bridge's terminal voltage $v_{TERM}(t)$ can be calculated from the voltages of the three connected armature windings $v_A(t)$, $v_B(t)$, $v_C(t)$. As seen in Figures 2.9 and 2.10, the difference between the highest and the lowest voltage forms the terminal voltage of the bridge.

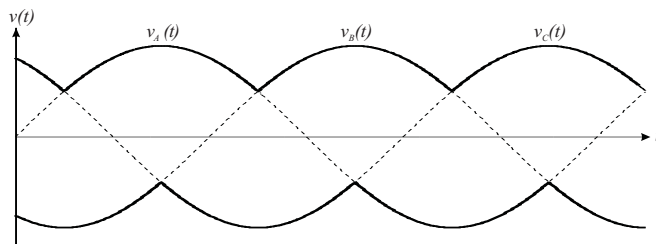


Figure 2.9: The highest and lowest voltages in a rectifier bridge

With three different potentials between the six diodes, current always flows from the highest of these potentials to the positive side of the circuit, and from the negative side of the circuit to the connection with the lowest potential.

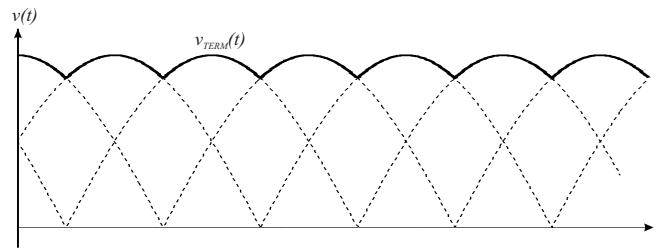


Figure 2.10: Terminal voltage of the rectifier bridge

2.2.4 Excitation Circuit and Control

To build the magnetic field around the rotor, a current is lead through the excitation winding, which is a part of the excitation circuit. This current is taken from the alternator's output current, making it self-excited. At low speeds, when not enough current is generated by the alternator to excite itself, current is taken from the battery. The current flows to the rotating excitation winding via a set up of carbon brushes and collector rings. To regulate the excitation current, and ultimately the whole alternator power output, the voltage over the excitation circuit is turned on and off. The switching is controlled by a pulse width modulated (PWM) signal, usually coming from the internal alternator regulator. The frequency and amplitude of a PWM signal is always the same, instead the duty cycle (on time) is controlled. A PWM with 50% duty cycle is a regular square wave, and has an on time as long as its off time. A PWM with 80% duty cycle is high 80% of a period, and low 20%. The average excitation current can thus be controlled by varying the duty cycle. A graph describing how the excitation current varies with the duty cycle can be seen in Figure 2.11.

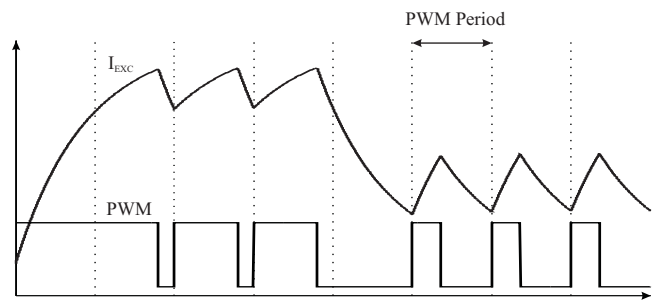


Figure 2.11: PWM signal and the corresponding excitation current

One of the advantages with a PWM controller is that it needs only one output pin to control the excitation circuit.

The internal regulator is usually subordinate to the master ECU controller. The ECU transfers parameters to the alternator regulator, which affects the control. These parameters are transferred via a LIN-interface. LIN (Local Interconnect Network) is a low-bandwidth, serial communication system for vehicles. It is used instead of CAN (Control Area Network) for low bandwidth applications.

A more thorough description of the alternator's different components can be found in [10].

2.3 Power Steering Pump

On the European market, power steering systems have existed since the 1950s [12]. When the driver turns the steering wheel, the power steering system is made to assist him if the turning is effortful (i.e. mainly at low speeds). The overall most common type are *hydraulic power assisted steering* (HPAS) systems, which use hydraulic oil flowing back and forward in a steering rack, thereby adding force to the steering. In small vehicles electric power steering systems have recently been introduced. This work will focus only on HPAS systems.

2.3.1 Servo System

The three important components in a HPAS system are

- Pump (power source)
- Servo valve
- Actuator

Whilst the pump provides a steady flow of pressurized oil, the servo valve distributes oil to the correct fluid line in correct amounts. The actuator is a piston system that helps push the steering rack in the direction wanted by the driver. A sketch of the system can be seen in Figure 2.12.

The flows to the steering rack chambers are controlled by a valve that is connected to the steering column. The amounts are decided by the steering wheel torque, where a boost curve [13] is used to map torque to pressure in the steering rack chambers. When help torque is needed to the steering, the hydraulic oil will flow through the valve to one of the chambers, thereby pushing a piston connected to the steering rack. The pressure difference needed to push this piston is obtained by letting the hydraulic pump work. The pump gets its power from the engine, and is just like the other auxiliary devices, mounted

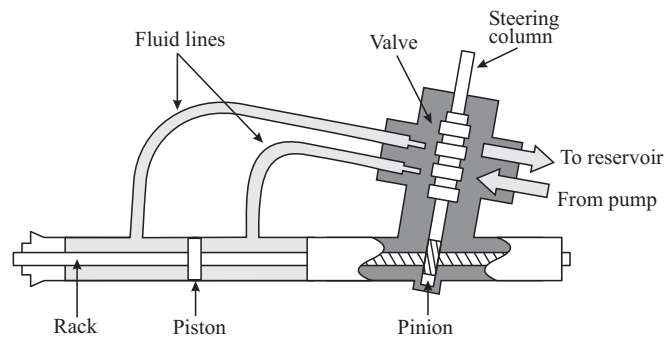


Figure 2.12: Power steering system (without the pump)

on the belt.

The valve of the servo system can be of either strictly hydromechanical type or of electro-hydraulic type. The former uses a set of pipes, integrated in the steering column to distribute the fluid to the chambers. The latter uses an electronic controller that can adapt the pressure need to the speed of the vehicle, as well as to the angle of the steering wheel. An electro-hydraulic converter is used to transfer the control signal between the two domains.

2.3.2 Power Steering Pump

The pump used for maintaining the hydraulic oil flow is of *rotary vane* type. It is connected to the valve at one end and to a hydraulic oil reservoir (often integrated with the pump) at the other. The oil is taken from the reservoir (suction side) and is brought to the outlet port via the pumping chambers. From the high pressure outlets of these chambers, oil is then available for the servo valve to distribute when help torque is needed.

The pumping mechanism uses a circular cylindrical rotor, or *vane house*, with a number of vanes, usually 10, in radial slits. These vanes are able to move radially in and out of the slits. The rotor is placed in the *pumping chamber*, with elliptic cylindrical geometry, with two inlets and outlets. As the rotor turns, the vanes will slide radially in their slits due to centrifugal force until they push against the inner walls of the pumping chamber. Between two consecutive vanes, a distinct volume of fluid can then be trapped in a hydraulic seal. During rotation this volume will be transferred from one side of the system to the other. The vane pump principle is illustrated in Figure 2.13. Modern systems use pairs of inlets and outlets, located 180 degrees apart. This port distribution gives equal and opposite side loads on the bearings that completely cancel each other, a configuration that significantly reduces wear.

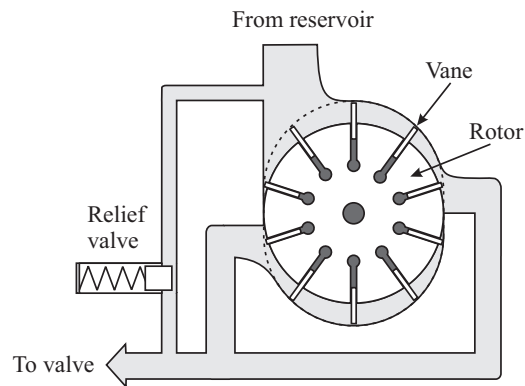


Figure 2.13: Rotary vane pump structure

To control the flow, a special type of throttling valve is used. This connects the reservoir and the pressurized channel. By closing or opening this valve, the feedback of high-pressurized hydraulic oil can be regulated. The pump control is of open loop type. This means that the ECU only send signals to the valve, it does not receive any. The control signal is of PWM type, with a low signal corresponding to a fully open and a high to a fully closed state. An electromagnet opens and closes the valve, and since magnetization is an inductive process and therefore not instantaneous, the PWM duty cycle will averagely correspond to the openness of the valve. In turn, this will correspond to the flow through it.

Chapter 3

Modelling Theory

There are several ways to model a system. Decisions about such things as complexity, method and simplifications to use have to be made. In this chapter, questions of this sort are discussed for the work at hand. A section describing stability tests is also included.

3.1 Complexity

Since the simulation environment is established as a HiL system by dSPACE, the model complexity has to be suited to the system. To be able to predict computation speed for each simulation step, the step-time has to be fixed. In order for it to run in real time, the whole model behaviour must be computable in real time, at each step. This must be valid for all possible states, regardless of the input signals.

The HiL system simulation step-time h is adapted to the existing engine and vehicle models, which run smoothly at this value. It is important that the added auxiliary devices models do not interfere with this set step-time, and thereby slow down other parts of the system. Thus, the ultimate real time tests must be done together with the engine and vehicle model in the HiL simulator. The simulation step-time h is in the magnitude of milliseconds. At the very least, the auxiliary devices models have to be suited to this time before final tests. A faster simulation guarantees smooth operation in the HiL simulator. The step-time is analogous to the sample time of the system, in the sense that it sets limits on the resolution. Events varying faster than h will not be visible in the final simulations.

However, much can be gained by starting with a complex model and simplifying that model to the low simulation step-time. Early high resolution

simulations can be done at a regular computer, using a modelled ECU in so called model-in-the-loop (MiL) tests. These simulations are used in the development process.

Processes varying very slowly (e.g. wear and tear), will not be modelled. Changes of this kind are not of interest in this work.

3.2 Method

When it comes to modelling method, one can choose between basing models on physics or using black box methods to build the models. Black box methods require much measurement data, and makes it virtually impossible to parametrize the models after physical properties. This work aims to make general models, useable with many different sizes and properties of the auxiliary devices. Therefore, using physics to describe and model the devices is the best choice for this work. Some areas could require the use of measured data and maps to simplify the physical description.

The working process will be to first find equations, usually ordinary differential equations (ODE:s), for the different parts of the systems and use these with one another to connect the subsystems. The modelling and simulation software SIMULINK from MATHWORKS will be used for this purpose. SIMULINK comes with many predefined system blocks for mathematics and system building and allows easy control over simulations. The software versions used are SIMULINK 5.0.2 and MATLAB 6.5. No extra toolboxes were used in the model building phase.

When a complete and complex physical description has been implemented for each system in SIMULINK, simulation tests to check the computation speed will be made using a regular computer at first and later the model will be integrated into the larger engine model, with real control signals from the ECU. To simulate the models with SIMULINK and in the HiL system, the differential equations are solved using numerical methods. In the HiL system, the final simulation environment, the *Euler method* is used. It will therefore be used throughout the modelling process. It is a rather simple and is shortly described as follows. From a state space description of the model

$$\begin{aligned}\dot{x}(t) &= f(x(t), u(t)) \\ x(0) &= x_0,\end{aligned}\tag{3.1}$$

with a known start value x_0 and an input signal $u(t)$, an approximation of the states at times t_1, t_2, \dots, t_n is desired. The easiest approximation of $\dot{x}(t)$ is

$$\frac{x_{n+1} - x_n}{h} \approx \dot{x}(t_n) = f(x_n, u_n),\tag{3.2}$$

where $h = t_{n+1} - t_n$ is the step time. This gives the equation

$$x_{n+1} = x_n + hf(x_n, u_n), \quad (3.3)$$

which is used during simulation to calculate the next simulation step. This method is more thoroughly described in [14], which is an overall good book on the subject of modelling and simulation. Another good source used in this work is [15].

In SIMULINK, a state description exists for each individual block. The state for each block is calculated for every step, but since blocks follow one another, with outputs from one block being the input for another, the order is also of great importance. During simulation initiation the blocks are therefore sorted according to the order in which they execute.

3.3 Stability

A model's quality is related to how well it can simulate the real system's behaviour, but also to the model's stability. The stability of a model is related to its ability to limit output from limited input. Small variations of input should result in small variations in output. A system is *asymptotically stable* when it is stable and solutions converge towards zero as $t \rightarrow \infty$. A homogenous linear system $\dot{x} = Ax$ is asymptotically stable when all eigenvalues of the matrix A have negative real parts.

For nonlinear systems, stability tests can be performed using *Lyapunov functions*, or by first linearizing the modelled system at an operating point, then using the above mentioned method with eigenvalues. Since the systems modelled in this work are real, and have limits on many of their signals, it is difficult to model them as linear systems. They are often piecewise linear though. In the MATLAB/SIMULINK environment the command `linmod` and its variants can be used to linearize the models created in SIMULINK, obtaining the state space matrices from the ODE:s.

The stability of a solution is however also affected by the numerical ODE solver. Using the chosen Euler algorithm, the stability of a system

$$\begin{aligned} \dot{x} &= \xi x, & \xi & \text{complex number} \\ x(0) &= 1, \end{aligned} \quad (3.4)$$

which can be solved with

$$x_{n+1} = x_n + h\xi x_n = (1 + h\xi)x_n, \quad (3.5)$$

and whose solution thus is

$$x_n = (1 + h\xi)^n, \quad (3.6)$$

is limited to the region where $|1 + h\xi| < 1$, the region within a circle of radius 1 and center in -1 [14]. This limits the simulation step-time h . The ξ term in these examples can be explained by the fact that for a regular ODE system $\dot{x} = Ax$ which is possible to formulate so that A is a diagonal matrix, one can find a diagonal containing the eigenvalues ξ . Consequently, the stability region for equation (3.4) will be the left half plane $\text{Re } \xi < 0$, differing from the stability region of the solver. This means that the differential equation in certain cases actually can be stable, but not the numerical solution of it.

Another way to investigate stability at different step sizes is simply to simulate the systems and find at what step-size they degenerate, or start to oscillate. A look on the systems' stability will be taken in chapter 5.2.

3.4 Validation

There are different approaches when validating models. The most desirable is of course to have a good data set of measurements to validate against. The validity can then be measured simply by comparing the measured data with a simulation of the same course of events. Mathematical measures like *mean absolute error* or *mean relative error* gives a tangible value of how good the models are.

Often though, the modelled structure does not exist in reality, or like in this work, there is a lack of measured data. This makes it hard to give an objective measure of the validity of the models. To analyse the validity there are a number of alternative approaches. If the model is based on previous work, there is a chance that work has been validated. From this validity, the validity of the new model can be deduced, but only to a certain extent.

Another kind of validation is to see that the modelled system really behaves like one could expect in different situations. Moreover, the lack of measured data does not mean a total lack of information. There is often a known range within which the phenomena, in this case torque, operates.

These methods requires a discussion about the validity of the system. A validity discussion about the auxiliary devices models can be found in chapter 6.3.

Chapter 4

Modelling

In this chapter models for the three devices are developed. The aim is as mentioned in Chapter 1, to model the torque of the auxiliary devices at different load situations, as well as the dynamic torque characteristics.

There are some similarities in the three devices. They are all mounted on the belt with pulleys of different size, and they all have rotational parts. The belt can be seen as stiff if belt dynamics are disregarded, a very common assumption. The pulleys merely transfer the engine speed ω_{eng} to the devices. The radius of the pulley r_{dev} in relation to the crankshaft pulley radius r_{cs} determines the factor the speed is multiplied as

$$p_{ratio,dev} = \frac{r_{dev}}{r_{cs}} \quad \omega_{dev} = p_{ratio,dev} \omega_{eng} \quad (4.1)$$

The auxiliary devices' total torques are related to the device specific internal torques (e.g. magnetic torque for the alternator, torque from friction for the AC compressor) but since the pulleys and the rotating bodies have certain masses and therefore also moments of inertia, these also add to the torques. According to newtonian mechanics, the moment of inertia J for a rotating body is related to the torque T as $T = J\dot{\omega}$. The torques thus relate to the moment of inertia as

$$J_{dev} \frac{d\omega}{dt} = T_{eng} - T_{dev} \quad (4.2)$$

The engine torque T_{eng} is adding to the system, while the device specific torque subtracts from it, thereby decreasing the available drive line torque.

Unfortunately, for this work, the engine torque signal was not available during all simulations. It was instead decided to drive the models with the engine speed signal. This changes the model structure to some extent. The need for integrative causality during simulation makes it impossible to simulate the

derivative of the input speed. The model structure used in the following is illustrated in the SIMULINK plot in Figure 4.1.

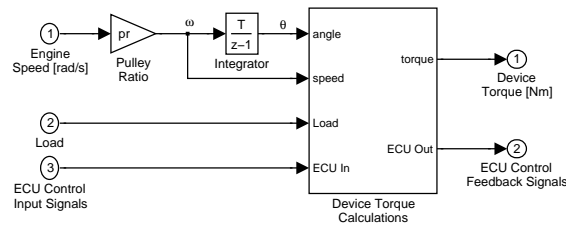


Figure 4.1: Model structure

This model structure removes the possibility to simulate the moment of inertia, which have the influence on the device torque that can be described as smoothing it, or slowing its dynamic. The mechanical moment of inertia are very similar to that of a flywheel for these devices. Another result of this decision is that possible influences on the device operation from the engine acceleration is not possible to model. It can be said that the models operates at a steady state engine speed.

4.1 AC Compressor

The main idea for the compressor modelling is to set up mechanical equations of how the pistons are moving, depending on swash plate angle and compressor speed. From this, the volume in the cylinders can be calculated at each point. The change in these volumes determine the compression, and the pressure at different points in time. This pressure exert forces against the swash plate which requires torque to counteract.

The torque of axial-piston swash plate machines have previously been described in [16], where a hydrostatic pump of this type was examined. The compressor model developed in this chapter is similar in many ways to this pump model, but the internal cylinder pressure is modelled differently in this work, since compression is the very essence of the machine.

4.1.1 Piston Kinematics

Most variables used in this chapter represent geometric quantities, and can be seen in Figure 4.2. A point x on one of the pistons, on a distance r from the middle axial position moves between displacement positions $x = r(\tan \alpha_{max} - \tan \alpha)$ and $x = r(\tan \alpha_{max} + \tan \alpha)$. The exact position of each piston depends on the angle difference between the piston centre φ_i and the top dead center (TDC) θ of the swash plate. The TDC is the angle

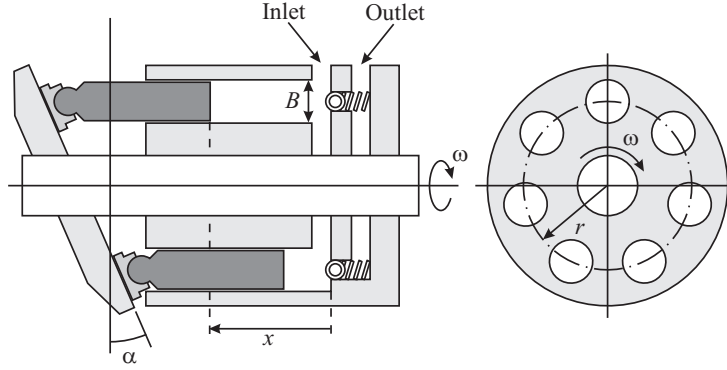


Figure 4.2: Swash plate mechanism

on the swash plate with maximum displacement (i.e. the angle at which the plate is tilted against). In Figure 4.2, the angle of the TDC and the top piston coincides. The position of piston i can be calculated as

$$x_i = r (\tan \alpha_{max} + \tan \alpha \cos(\theta - \varphi_i)) \quad (4.3)$$

Differentiating this equation, the velocity of each piston can thus be calculated as

$$\dot{x}_i = -r \omega \tan \alpha \sin(\theta - \varphi_i) \quad (4.4)$$

where $\omega = \dot{\theta}$ is the speed of rotation for the compressor. Similarly, the acceleration of each piston is expressed as

$$\ddot{x}_i = -r \omega^2 \tan \alpha \cos(\theta - \varphi_i) \quad (4.5)$$

The cylinder volume is totally dependant on the piston position. With a circular piston area, and the cylinder diameter B , the piston area $A_p = \frac{1}{4}\pi B^2$. If the swash plate angle is held constant during a revolution, and no refrigerant leakages are considered, the total displacement volume V_G during this revolution, the *geometric displacement volume*, will be

$$V_G = A_p N 2r \tan \alpha \quad (4.6)$$

where N is the number of cylinders in the compressor. This refrigerant volume is of course a volume at suction pressure. The instantaneous volume for piston i is

$$V_i = A_p r (\tan \alpha_{max} + \tan \alpha \cos(\theta - \varphi_i)) \quad (4.7)$$

On each piston there are forces aligned with the piston's movement due to friction against the cylinder walls, by acceleration of the piston mass m_p and

by the compressed refrigerant. The friction will for now be neglected. The acceleration of the piston exerts a force of size $m_p \ddot{x}_i$ on the piston itself, according to Newton's second law. This force is especially significant at high speeds and with few cylinders in the compressor. The refrigerant pressure inside the cylinder exerts a force on the piston that is depending on the pressure p_i and the piston area A_p . Summing these forces gives the total force on piston i

$$F_i = m_p \ddot{x}_i + A_p p_i \quad (4.8)$$

in the positive x direction of Figure 4.2.

4.1.2 Adiabatic Process

To calculate the instantaneous pressure in each cylinder the volume and mass of the refrigerant are used. The refrigerant (R-134a) is in its gaseous form in the compressor. The working pressures ranges from 2 to 24 atm (200 kPa - 2.4 MPa). If no refrigerant or heat flows in or out of the cylinder during compression, it can be modeled like an adiabatic process. In reality heat will flow through the cylinder walls, and this could lead to modelling errors. A discussion about errors follows in Chapter 6. For a adiabatic and reversible process, the relation between pressure and specific volume is described by

$$pV^\gamma = C \quad (4.9)$$

where γ and C are constants. Using data sheet figures [17], these two constants are calculated using the least squared error approach. This is because the data gives an over-determined equation system. Logarithms of equation (4.9) gives

$$\ln(p) + \gamma \ln(V) = \ln(C) \quad (4.10)$$

which can be rewritten on the form

$$\begin{cases} \ln(V_1)\gamma - \ln(C) = -\ln(p_1) \\ \ln(V_2)\gamma - \ln(C) = -\ln(p_2) \\ \vdots \\ \ln(V_m)\gamma - \ln(C) = -\ln(p_m) \end{cases} \quad (4.11)$$

where m is the number of data points used to determine the values. This system can be written as

$$\mathbf{Ax} = \mathbf{b} \quad (4.12)$$

with

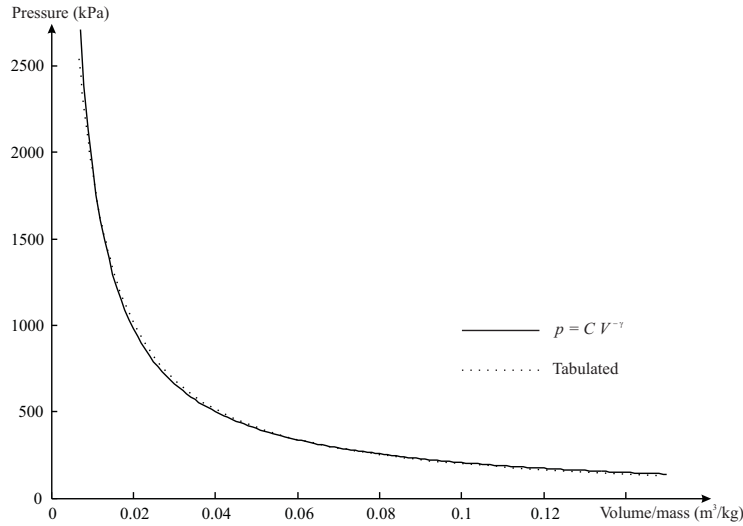


Figure 4.3: Comparison between tabulated values and (4.14)

$$\mathbf{A} = \begin{pmatrix} \ln(V_1) & 1 \\ \ln(V_2) & 1 \\ \vdots & \vdots \\ \ln(V_m) & 1 \end{pmatrix} \quad \mathbf{x} = \begin{pmatrix} \gamma \\ -\ln(C) \end{pmatrix} \quad \mathbf{b} = \begin{pmatrix} -\ln(p_1) \\ -\ln(p_2) \\ \vdots \\ -\ln(p_m) \end{pmatrix} \quad (4.13)$$

This equation system can be easily solved in MATLAB using the `\` operator like `A\b`. This operator gives the solution in the least square sense to the over-determined system of equations (4.12), avoiding numerical problems by employing QR decomposition techniques.

Using $m = 100$ measurement points, distributed over the working pressure, to decide the two constants, the results are $\gamma = 0.9695$ and $C = 22088$. Applying these estimates in equation (4.9), the pressure of the refrigerant can be calculated when the specific volume is known

$$p = C V^{-\gamma} \quad (4.14)$$

This pressure affects the pistons directly as forces in axial direction during compression. One could argue that the lookup table could be used directly instead of using a table to approximate physical properties. However, as can be seen in Figure 4.3, a comparison between values from (4.14) and the tabulated values, the adiabatic process estimation is rather good.

4.1.3 The Compression Cycle

The use of equation (4.14) is only permitted in a closed cylinder, without mass flows. However, these occur at certain points during a compression cycle.

As the pistons goes back and forth in the cylinders, they go through a suction phase and through a compression phase. During the compression phase, they move forwards (negative x direction in Figure 4.2). When they move backwards, the cylinders take in low-pressure refrigerant; this is the suction phase. This is a mass flow. During this phase, the pressure in the cylinder will be the same as the low-pressure p_l of the uncompressed refrigerant or, when some refrigerant from the foregoing cycle remains in the cylinder, it will follow the polytropic curve in figure 4.3 but towards a lower pressure. The low-pressure p_l is constant, determined by the systems expansion valve.

Moreover, the compressed refrigerant leaves the cylinder when a certain pressure has been achieved. The control of this is through the pressure-relief valve. The discharge pressure p_r is set from the start as a parameter of the valve. As the compression continues the refrigerant will remain at this pressure which lets it flow through the valve. The typical chatter of these types of valves will not be modelled in this work.

The new pressure function will be

$$p(V) = \begin{cases} p_l & \frac{dV}{dt} > 0 \\ C V^{-\gamma} & \\ p_r & C V^{-\gamma} > p_r \end{cases} \quad (4.15)$$

4.1.4 Deduction of Torque

The total axial force on each piston F_i , must be overcome by a reaction force R_i to move it. This reaction force act on the piston from the swash plate. It is perpendicular to the contact area between them. The component of this force perpendicular to the piston movement and its distance from the center of the swash plate acts as a moment arm and transmits the torque T_i to each piston, overcoming the axial forces and making the machine run. The geometries and forces are illustrated in Figure 4.4.

The swash-plate reaction force R_i is related to F_i as

$$R_i \cos \alpha = F_i = m_p \ddot{x}_i + p_i A_p \quad (4.16)$$

To move the machine, the torque produces the component of R_i perpendicular to the piston movement. This component is $R_i \sin \alpha$ and with a moment arm of $r \cos(\theta - \varphi_i)$ the torque

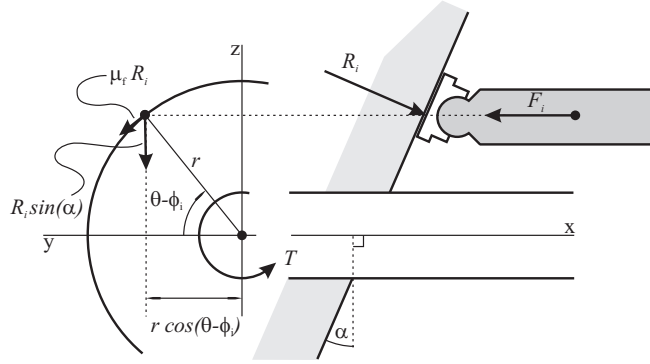


Figure 4.4: Forces acting on the swash plate from a single piston.

$$T_i = R_i \sin \alpha r \cos(\theta - \varphi_i) \quad (4.17)$$

is needed for every piston i . Combining (4.16) and (4.17) as well as summing the components from all pistons, the torque is

$$T = \sum_{i=1}^N (m_p \ddot{x}_i + p_i A_p) \tan \alpha r \cos(\theta - \varphi_i) \quad (4.18)$$

Furthermore, it is possible to calculate an approximation of torque due to friction between the piston slipper and the swash plate. An expression for the reaction force already exists in (4.16) and since this is the force perpendicular to the contact areas, this is also the force giving rise to friction. With a linear friction assumption, a force of size $\mu_f R_i$ will act for each piston on the distance r from the shaft center. Summing up this for all the pistons, the torque due to friction becomes

$$T_f = \frac{r}{\cos \alpha} \sum_{i=1}^N m_p \ddot{x}_i + p_i A_p \quad (4.19)$$

Friction is often disregarded when modelling moving mechanical systems like this, but in this case it is a simple matter to calculate a friction estimate, and it can therefore be interesting to see how much of the total torque it constitutes.

4.1.5 Mass Flow and Control

To determine the efficiency of the compressor, it is necessary to know the amount of refrigerant flowing through it. This mass flow can be calculated at the output side of the compressor. During each revolution, a certain amount of refrigerant is compressed and passes the pressure relief valve. The mass flow is directly related to the swash plate angle since this decides the stroke

volume in the compressor. If the pistons are able to compress the refrigerant and heighten the pressure enough for it to overcome the spring force in the relief-valve (this is not always the case), the refrigerant mass passing the valve during one revolution will be the difference $V_g - N V_r$, where V_r is the volume at which the pressure p_r is reached.

$$V_r = \left(\frac{C}{p_r} \right)^{\frac{1}{\gamma}} \quad (4.20)$$

By multiplying the mass flow per revolution with the revolutions per second, we get the mass flow per time unit.

$$Q = 2\pi \omega (V_g - N V_r) \quad (4.21)$$

Fluid power can be derived directly from this expression as the mass flow times the pressure increase $P = (p_r - p_l) Q$.

The real compressor is affected by three ECU:s, the engine ECU (which is the target control unit for this whole work), the AC ECU and the coupé ECU. Unfortunately the detailed description for the two latter was missing during this work. These two control most of the AC system, the engine only sets some prescribed maximum values for some of the compressor's signals (e.g. the torque).

To model the control system, it is in this work assumed that the thermal control signal is directly linked to the fluid power. The controller gets its set point as a percentage of maximum power, a manual input to the system. The control signal is fed back to the swash plate, and controls its angle. The dynamics of the swash plate angle is modelled using a simple first order model.

4.2 Alternator

Previously, physical models of claw pole alternators have been constructed in different ways. There are complex approaches using finite elements methods (FEM) [18, 19], and there are very simple models [15]. In this text a middle course is taken, the alternator is modelled like a synchronous machine with simplified magnetic characteristics. A similar approach has been taken in [20].

The idea is to find equations for the different parts of the alternator and simulate and solve them with one another. The main components will be the rotor, the stators, the rectifier bridge and the regulator. A separate set of equations will be used to calculate the torque.

4.2.1 Rotor

Excluding the torque due to moment of inertia, the alternator torque mainly consists of magnetic fields pulling at the rotor, magnetic torque. To calculate this variable, the different electric and magnetic quantities must be simulated.

Even though the rotor is of claw pole type it can be approximated as a synchronous machine. This has been done before in [20], and the approximation is valid since the poles rotate as salient poles. The excitation winding though, does not rotate in the same way as in normal salient pole machines. This gives the advantage of it not cutting the field lines from the magnetic field generated by the stator windings. The excitation current is therefore hardly affected by the armature flux wave. A simple sketch of the rotor's electric equivalent is shown in Figure 4.5.

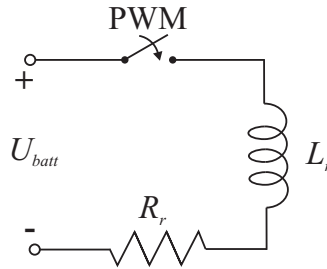


Figure 4.5: Rotor circuit

The resistance of the excitation circuit is R_r and the inductance L_r . To calculate the excitation current i_{exc} flowing through this circuit, Kirchoff's voltage law (KVL) is used with the battery voltage U_{batt} and the resulting differential equation

$$L_r \frac{di_{exc}}{dt} + R_r i_{exc} = U_{batt} \quad (4.22)$$

must be solved. The rotor inductance L_r can be described by $L_r = L_{lr} + L_{mr}$ where the two terms L_{lr} and L_{mr} are the rotor *leakage inductance* and the rotor *magnetizing inductance*. The excitation current controls how much power the system generates.

All poles on the rotor share the same excitation winding, but the number of poles is significant to how fast the system works. The difference between a two pole machine and a four pole machine has only to do with the speed they operate. A two pole machine generates magnetic fields at the stators synchronized with the mechanical speed, thereby one rotation by the rotor will translate to one period in the field at the armature. However, if the number

of poles on the rotor are higher, the electric speed will be faster. Therefore it is convenient, whenever working with a multiple pole machine to make the conversion from mechanical angles and speeds θ_m, ω_m to electrical angles and speeds θ, ω . For a machine with P poles

$$\begin{aligned}\theta &= \frac{P}{2}\theta_m, & \text{and} \\ \omega &= \frac{P}{2}\omega_m\end{aligned}\quad (4.23)$$

This simplifies calculations considerably. One can analyze the system like for a two pole machine, the only difference is the speed.

4.2.2 Magnetic Field

To quantitatively determine the generated voltages in the armature (stator) windings, a more thorough discussion about the magnetic flux is needed.

The field winding on the rotor can be assumed to produce a sinusoidal magnetic flux wave of density B at the armature windings.

$$B = B_{peak} \cos \theta \quad (4.24)$$

The air-gap flux per pole Φ is the integral of the flux density over the pole areas. For a P -pole machine with pole areas symmetrically distributed over the stator housing

$$\Phi = \int_{-\pi/P}^{+\pi/P} B_{peak} \cos \frac{P}{2}\theta lr \, d\theta = \frac{2}{P} 2B_{peak}lr \quad (4.25)$$

where l is the axial length of the stator and r is its radius at the air gap. A P pole machine has pole areas that are $2/P$ times that of a two pole machine of the same size.

$$\Phi = \frac{2}{P} 2B_{peak}lr \quad (4.26)$$

The flux linkage λ for a stator winding with N turns will vary as

$$\lambda = N\Phi \cos \omega t \quad (4.27)$$

where ωt represents the angle between the magnetic axes of the stator winding and the rotor. The time t can be chosen so that at $t = 0$ the peak of the flux density wave coincides with the magnetic axis of one of the stator windings. Faraday's law is then applicable to calculate the induced voltage in each phase winding as

$$V = \frac{d\lambda}{dt} = N \frac{d\Phi}{dt} \cos \omega t - \omega N \Phi \sin \omega t \quad (4.28)$$

This equation also applies where Φ is the net air-gap flux per poles, produced by currents in both the stator and the rotor windings. There are two terms in the equation. The first one is a transformer voltage and exists only when the amplitude of the flux-density wave changes with time, normally this does not happen in a well balanced system running in steady state. The second term, often called the speed voltage, or electromotive force (EMF), is thus in most cases the one that dominates the generated voltage.

In steady state operation the EMF will hereafter be used to represent the generated voltage

$$V = -\omega N \Phi \sin \omega t \quad (4.29)$$

This voltage is laid over each armature winding as the rotor turns and magnetic fields are excited.

4.2.3 Armature Windings

The armature windings can be approximated with inductances in series with a resistance. As the rotor turns and magnetic fields are produced, the induced voltages will produce currents through these windings. The currents through the windings in turn also affect the flux linkages. The flux linkage from the rotor together with the flux linkage from the self-inductance of each winding, and that from the mutual inductances of the other windings sums up to a total flux linkage. If \mathcal{L}_{xy} denotes the mutual inductance between winding x and y , the flux linkages can be described as

$$\begin{aligned} \lambda_a &= \mathcal{L}_{aa}i_a + \mathcal{L}_{ab}i_b + \mathcal{L}_{ac}i_c + \mathcal{L}_{ar}i_r \\ \lambda_b &= \mathcal{L}_{ba}i_a + \mathcal{L}_{bb}i_b + \mathcal{L}_{bc}i_c + \mathcal{L}_{br}i_r \\ \lambda_c &= \mathcal{L}_{ca}i_a + \mathcal{L}_{cb}i_b + \mathcal{L}_{cc}i_c + \mathcal{L}_{cr}i_r \end{aligned} \quad (4.30)$$

where the term \mathcal{L}_{xr} are the angle-dependant mutual inductances between rotor and stator. The three armature windings are constructed equal and should possess equal physical properties. They are also symmetrical, and owing to this, the stator-stator mutual inductances \mathcal{L}_{xy} , $x \neq y$ will all be of the same size, L_{ss} which in turn can be expressed using the stator magnetizing inductance L_{ms} as $L_{ss} = L_{ms} \cos \frac{2\pi}{3} = -\frac{1}{2}L_{ms}$ due to the winding phase distribution of $\frac{2\pi}{3}$ radians. The self-inductance of the windings, $\mathcal{L}_{xx} = L_s = L_{ms} + L_{ls}$ is the sum of the stator magnetizing inductance and the stator leakage inductance. Thus, equations (4.30) become

$$\begin{aligned}
\lambda_a &= L_s i_a + L_{ss} i_b + L_{ss} i_c + \mathcal{L}_{ar} i_r \\
\lambda_b &= L_{ss} i_a + L_s i_b + L_{ss} i_c + \mathcal{L}_{br} i_r \\
\lambda_c &= L_{ss} i_a + L_{ss} i_b + L_s i_c + \mathcal{L}_{cr} i_r
\end{aligned} \tag{4.31}$$

It is easily understood that the three stator currents sum up to zero

$$i_a + i_b + i_c = 0 \tag{4.32}$$

which with the relations for L_s and L_{ss} can be used to further simplify (4.31) to

$$\begin{aligned}
\lambda_a &= \left(\frac{1}{2}L_{ms} - L_{ls}\right)i_a + \mathcal{L}_{ar} i_r \\
\lambda_b &= \left(\frac{1}{2}L_{ms} - L_{ls}\right)i_b + \mathcal{L}_{br} i_r \\
\lambda_c &= \left(\frac{1}{2}L_{ms} - L_{ls}\right)i_c + \mathcal{L}_{cr} i_r
\end{aligned} \tag{4.33}$$

The $\mathcal{L}_{xr} i_r$ terms corresponds to the flux linkage generated from the field winding, as described in equation (4.27). The \mathcal{L}_{xr} terms are angle-dependent, but its amplitude is often described with the *peak stator-rotor mutual inductance* variable L_{sr} which can be broken down into $L_{sr} = k\sqrt{L_{mr}L_{ms}}$. Here, k is the stator-rotor coefficient of magnetic coupling, a measurement of how good the magnetic field transfers between rotor and stator.

An electric schematic of the armature windings can be seen in Figure 4.6. The diamond shaped boxes represent the derivative of the flux linkages over that winding, equation (4.33), meaning a container for a voltage source and an inductance.

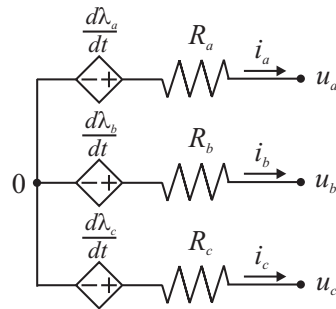


Figure 4.6: Stator circuit

For an alternating current system, lacking the rectifier bridge, KVL for this system yields the system of equations

$$\begin{aligned}\frac{d\lambda_a(t)}{dt} &= u_a(t) - R_s i_a(t) \\ \frac{d\lambda_b(t)}{dt} &= u_b(t) - R_s i_b(t) \\ \frac{d\lambda_c(t)}{dt} &= u_c(t) - R_s i_c(t)\end{aligned}\quad (4.34)$$

where the voltages u_a , u_b and u_c represent the voltages at the three terminals of the armature Y-connection, and R_s is the winding resistance, equal for the three windings in concordance with the equality argument above.

This is a good description for a detached Y-connection. For the system at hand however, there is a three-phase bridge connected to the three terminals. The functionality of the rectifier bridge is described in chapter 2.2.3. The diode configuration only allows current to flow through two of the windings at once. The ones with maximal and minimal u voltages. The maximal and minimal u are determined by the maximal and minimal $\frac{d\lambda}{dt}$, and if the diode resistances in the forward direction is disregarded (i.e. the diodes are considered ideal), these will correspond to the battery voltage U_{batt} and ground. The two stator winding currents will be equal in magnitude, but with opposite signs.

The electric system simulated can be seen in Figure 4.7. Notice that the current and voltage source directions correspond two those in Figure 4.6.

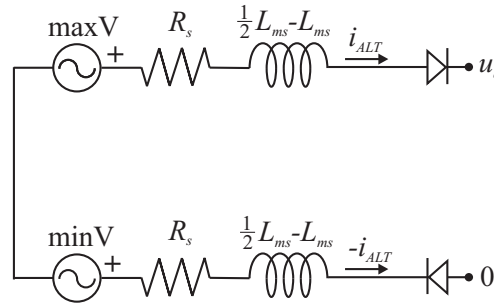


Figure 4.7: Full equivalent stator circuit

The simplification demonstrated in Figure 4.7 includes the diode bridge and the diodes shown does only imply the connection spots of the circuit, and shall not be taken into calculation.

In parallel to the diode bridge, it is common to put a capacitor, which functions to adjust the output current to a smoother signal. This capacitor is not modelled due to causality conflicts.

4.2.4 Torque

The electromagnetic torque on the rotor comes from the interacting magnetic field from the rotor circuit and the stator circuit. It can be expressed [11] like

$$T = -L_{sr} \left(\frac{P}{2} \right) i_{exc} i_s \sin \delta \quad (4.35)$$

where i_s denotes the current flowing through the stator windings, L_{sr} is the peak stator-rotor mutual inductance and δ the displacement angle of the two rotating fields. In deciding this angle, it is important to sum up the magnetic axes from the two active stator windings and compare the angle of this axis to that of the rotor magnetic field axis.

4.3 Power Steering Pump

Modelling complex hydraulic systems usually requires the use of Navier-Stokes equations, whose complexity stretches beyond what is possible in this work. Smaller models of these kinds of pumps are usually very simple, and does not account for in-cycle behaviour. Since the power steering pump is not very controllable, a simple averaging model of its torque could suffice. Such a model is presented in section 4.3.1. Moreover, in the following sections, the in-cycle behaviour is investigated by a model based on instantaneous flow, pressure and fluid characteristics inside the pumping chamber. Many of the ideas presented in section 4.3.4 comes from [16].

4.3.1 Simple Model

Looking at the power of a pumping system in a macro input-output perspective, the steady-state hydraulic power \dot{W}_{hyd} delivered by the pump can be described by

$$\dot{W}_{hyd} = V_p \omega (p_r - p_l), \quad (4.36)$$

where V_p is the *volumetric displacement* of the pump, and p_r , and p_l are the discharge pressure and the intake pressures [16]. From the rotation the input mechanical power to the system is

$$\dot{W}_{mec} = T \omega \quad (4.37)$$

By combining equation (4.36) and (4.37), and introducing an efficiency parameter η , a static relation between input power and output power becomes

$$\dot{W}_{hyd} = \eta \dot{W}_{mec} \quad (4.38)$$

Simplified, this relates the torque to the pump variables

$$T = \frac{1}{\eta} V_p (p_r - p_l) \quad (4.39)$$

Equation (4.39) does unfortunately not say anything about the dynamics of the torque. In the next section, an attempt to expand this model is made.

4.3.2 Vane Dynamics

The pumping chamber has elliptic cylindric geometry, within which the circular cylindric rotor, or vane house rotates. The geometries are further described in Figure 4.8.

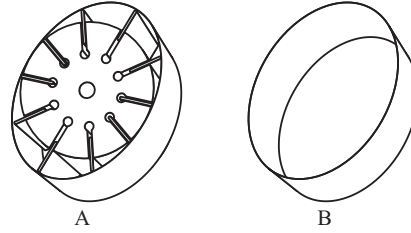


Figure 4.8: Geometries of the system. A) The rotor (vane house) inside the pumping chamber, B) The elliptic geometry of the pumping chamber.

The different geometric variables are designated in Figure 4.9 which gives a more detailed description of the system. The open area between ϕ_1 and ϕ_2 is one of the inlets of the pump, the outlet is between angles ϕ_3 and ϕ_4 . The other side of the pump is similar, only upside down.

The cranking vane house is always circular cylindric and can independently of the geometry of the pumping chamber be described by the radius L_1 , the depth b_l and the number of sliding vanes N . The pumping chamber can, taking a elliptic cylindric approach be described by the length L_2 of the semi-major axis, and the length L_1 of its semiminor axis, which it shares with the rotor. The depth is b_l for the pumping chamber as well. In the following calculations the coordinate system is aligned so that the pump house is skewed vertically with the vane house.

The edge of an ellipse can be represented by the parametrisation

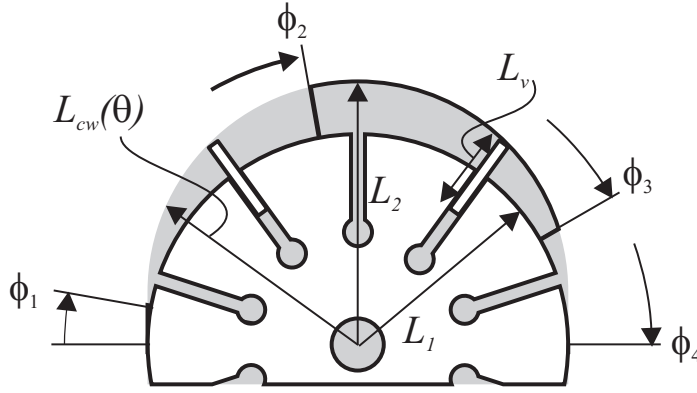


Figure 4.9: Vane House Detail

$$\begin{aligned} x &= -L_1 \cos \theta \\ y &= L_2 \sin \theta, \quad 0 \leq \theta < 2\pi \end{aligned} \quad (4.40)$$

The length from the origin, or in this case the joint center of the rotor and the pumping chamber, to the inner wall of the chamber is thus

$$L_{cw}(\theta_i) = \sqrt{L_1^2 - (L_1^2 - L_2^2) \sin^2 \theta_i} \quad (4.41)$$

with θ being the angle from the vertical axis to the point of interest, in the following to the vane of index i . This formula comes from Pythagoras' theorem, with a trigonometric law applied to give this form.

The friction between the vanes and the pumping chamber is dependent on the force with which the vanes press against the inner chamber wall. This force is due to the centrifugal force, and can be calculated from Newton's second law of motion.

Assuming the friction between the rotor and the vanes are small, the vanes will, due to the centrifugal force, be at their maximal displacement. The center of mass of the vanes will therefore move in a curve, in a polar coordinate system described by

$$\mathcal{R}(\theta_i) = \left(L_{cw}(\theta_i) - \frac{L_v}{2} \right) \hat{r} \quad (4.42)$$

where L_v is the vane length, and it is assumed that the vanes are rectangular in all directions, with solid mass distribution over their volume. Formulas for bodies moving in polar coordinate systems can be found in [21] and rotating motion is describable by

$$\begin{aligned}
x &= r \hat{r} \\
\dot{x} &= \dot{r} \hat{r} + r \dot{\theta} \hat{\theta} \\
\ddot{x} &= (\ddot{r} - r \dot{\theta}^2) \hat{r} + (r \ddot{\theta} + 2 \dot{r} \dot{\theta}) \hat{\theta}
\end{aligned} \tag{4.43}$$

To determine the radial acceleration described above, the derivatives of the radial component $\mathcal{R}(\theta)$ can be calculated to

$$\begin{aligned}
\dot{\mathcal{R}}(\theta) &= -\dot{\theta} \frac{(L_1^2 - L_2^2) \sin \theta \cos \theta}{\sqrt{L_1^2 - (L_1^2 - L_2^2) \sin^2 \theta}} \\
\ddot{\mathcal{R}}(\theta) &= -\dot{\theta}^2 \left[\frac{(L_1^2 - L_2^2)(\cos^2 \theta - \sin^2 \theta)}{\sqrt{L_1^2 - (L_1^2 - L_2^2) \sin^2 \theta}} + \frac{(L_1^2 - L_2^2)^2 \cos^2 \theta \sin^2 \theta}{(L_1^2 - (L_1^2 - L_2^2) \sin^2 \theta)^{\frac{3}{2}}} \right] \\
&\quad + \ddot{\theta} \frac{(L_1^2 - L_2^2) \sin \theta \cos \theta}{\sqrt{L_1^2 - (L_1^2 - L_2^2) \sin^2 \theta}}
\end{aligned} \tag{4.44}$$

For a steady-state system, the $\ddot{\theta}$ term is zero and this term can thus be disregarded. Using (4.44) with the component for radial acceleration in equation (4.43), the following expression describes the radial acceleration a_v of the vanes in the vane pump

$$a_v(\theta_i, \dot{\theta}_i) = \ddot{\mathcal{R}}(\theta_i) - \mathcal{R}(\theta_i) \dot{\theta}_i^2 \tag{4.45}$$

Together with the individual vane masses m_v , an expression for the radial forces can be obtained using Newton's second equation. These forces will result in friction. For a linear friction approximation, these will be of size

$$F_{fi} = \mu_f m_v a_v \tag{4.46}$$

These friction forces will result in a torque component T_f , which will be

$$T_f(\theta, \dot{\theta}_i) = \mu_f m_v \sum_N L_{cw}(\theta_i) a_v(\theta_i, \dot{\theta}_i) \tag{4.47}$$

A linear friction model has been used here, with a constant μ_f . More advanced techniques of modelling friction, like *Stribeck curves* [22], are possible to implement but finding parameters for the frictional curve is much harder. For linear sliding friction on a lubricated surface, typical values of μ_f are between 0.01 and 0.1 for steel/steel contact areas [21].

4.3.3 Hydraulic Seal

As the vane house rotates, a hydraulic seal will be created between two consecutive vanes. The volume of this seal can be calculated from the lengths defined. With two vanes, on angles θ_1 and θ_2 respectively, the volume V_{12} between the two will be

$$V_{12} = b_l \int_{\theta_1}^{\theta_2} \int_{L_1}^{L_{cw}(\theta)} r dr d\theta \quad (4.48)$$

Which can be solved quite easily

$$\begin{aligned} V_{12} &= \frac{b_l}{2} \int_{\theta_1}^{\theta_2} L_{cw}^2(\theta) - L_1^2 d\theta = \frac{b_l}{2} (L_2^2 - L_1^2) \int_{\theta_1}^{\theta_2} \sin^2 \theta d\theta = \\ &\frac{b_l}{4} (L_2^2 - L_1^2) \left[(\theta_2 - \theta_1) - \frac{1}{2} (\sin 2\theta_2 - \sin 2\theta_1) \right] \end{aligned} \quad (4.49)$$

The angle between any two vanes is constantly $\theta_{i+1} - \theta_i = \frac{2\pi}{N} = \Delta_N$. This and further trigonometric simplifications of (4.49) leads to the general expression

$$V_{i,i+1} = \frac{b_l}{4} (L_2^2 - L_1^2) [\Delta_N - \sin \Delta_N \cos(2\theta_i + \Delta_N)] \quad (4.50)$$

This equation is static during simulation, making it a simple mapping $\theta \mapsto V$. The volume between vanes is reduced between the inlet orifices of the pump and the outlets, this means that the hydraulic fluid is compressed. The rate change of this compression, or the volume change is

$$\frac{dV_{i,i+1}}{dt} = \frac{b_l \omega}{2} (L_2^2 - L_1^2) \sin \Delta_N \sin(2\theta_i + \Delta_N) \quad (4.51)$$

The instantaneous pressure inside the hydraulic seals can be calculated from the volume of the hydraulic seal and the inlet and outlet characteristics.

4.3.4 Fluid Dynamics

Inside one of these hydraulic seals the instantaneous mass is given by $M = \rho V$, where ρ is the mass density, varying with time. The mass flow is given by the derivative

$$\frac{dM}{dt} = \frac{d\rho}{dt} V + \rho \frac{dV}{dt} \quad (4.52)$$

Within each seal, the mass remains constant, which means that

$$\frac{dM}{dt} = \rho Q \quad (4.53)$$

where Q is the volumetric flow rate into the hydraulic seal at the inlet. The definition of fluid bulk modulus [23] β gives the relation

$$\frac{d\rho}{dt} = \frac{\rho}{\beta} \frac{dp}{dt} \quad (4.54)$$

where p is the instantaneous pressure in the hydraulic seal. It is assumed that this is uniformly distributed over the whole seal volume. By inserting equations (4.53) and (4.54) into (4.52), and rearranging terms, the pressure derivative will be

$$\frac{dp}{dt} = \frac{\beta}{V} \left(Q - \frac{dV}{dt} \right) \quad (4.55)$$

Assuming the flow into and out of the pump have high speeds, the flow can be modelled using the orifice equation and Torricelli's principle [23]

$$Q = C_d A_b \sqrt{\frac{2|p_b - p|}{\rho}} \quad (4.56)$$

which will be negative at the inlet and positive at the outlet. Using the sign function $\text{sign}(p_b - p)$ for this is useful, p_b is the boundary pressure outside of the hydraulic seal, i.e. it is either the intake or the discharge pressure. The parameter C_d is the orifice discharge coefficient, and A_b is the active inlet or outlet area, varying with the angle.

Using equation (4.55) with (4.56) and the expression for the volume time derivative in (4.51), the nonlinear differential equation

$$\frac{dp_i}{d\theta} = \frac{\beta \left(\frac{\text{sign}(p_b - p_i) C_d A_b}{\omega} \sqrt{\frac{2|p_b - p_i|}{\rho}} + \frac{b_l}{2} (L_2^2 - L_1^2) \sin \Delta_N \sin(2\theta_i + \Delta_N) \right)}{\frac{b_l}{4} (L_2^2 - L_1^2) [\Delta_N - \sin \Delta_N \cos(2\theta_i + \Delta_N)]} \quad (4.57)$$

describes the pressure inside one hydraulic seal. Instead of writing this as a time dependent system, it is here written with the use of the valid substitution $dt = d\theta/\omega$. The pressure varies with the angle of the hydraulic seal, and therefore this seems natural. This system can be solved numerically using MATLABs ODE solver, or by constructing it with SIMULINK. A solution between angles 0 and π , one of the two pumping chambers, is presented in Figure 4.10

As can be seen, the pressure is smooth when in contact with the intake or discharge ports. The transition between them is seemingly linear, and a common assumption [16] is to make a simpler model of the pressure where

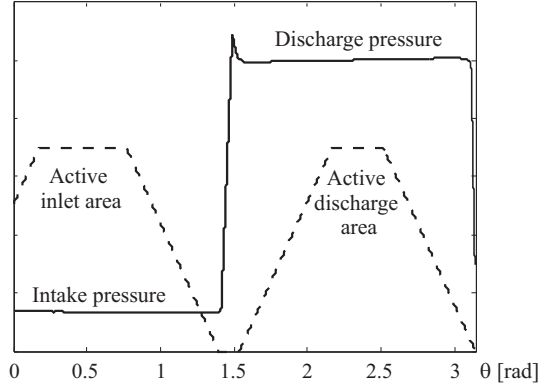


Figure 4.10: Pressure characteristics for one hydraulic seal $0 \leq \theta < \pi$

$$p_b = \begin{cases} p_l & 0 < \theta < \phi_2 \\ p_l + (\theta - \phi_2) \frac{p_r - p_l}{\phi_3 - \Delta_N - \phi_2} & \phi_2 < \theta < \phi_3 - \Delta_N \\ p_r & \phi_3 - \Delta_N < \theta < \pi \end{cases} \quad (4.58)$$

4.3.5 Torque

On a vane separating two seals two pressures will act on the two sides of the vane. The pressure difference will result in forces on both sides according to Figure 4.11. The modelled pressure profile of the pump (4.58) or Figure 4.10 indicates that this is only of great importance close to the inlet or outlet ports.

The forces acting on the vanes during rotation is described in Figure 4.11. For each vane i , the force on its front side (the one pushing the fluid) will be

$$F_{ii} = p_i b_l (L_{cw}(\theta_i) - L_1), \quad (4.59)$$

where $b_l (L_{cw}(\theta_i) - L_1)$ is the active vane area, the area the pressure is applied upon. On the back side of the vane, the force $F_{i-1,i}$ will act. If the vanes are considered thin, the front side and its back side have the same area. Since

$$F_{i-1,i} = p_{i-1} b_l (L_{cw}(\theta_i) - L_1), \quad (4.60)$$

and the both forces act on the same point, but in different directions, they add up to a net force

$$F_i = (p_i - p_{i-1}) b_l (L_{cw}(\theta_i) - L_1), \quad (4.61)$$

on each vane. This force is always positive ($p_i > p_{i-1}$) and adds to the torque due to its moment arm. The length of the moment arm is $\frac{1}{2}(L_1 + L_{cw}(\theta_i))$

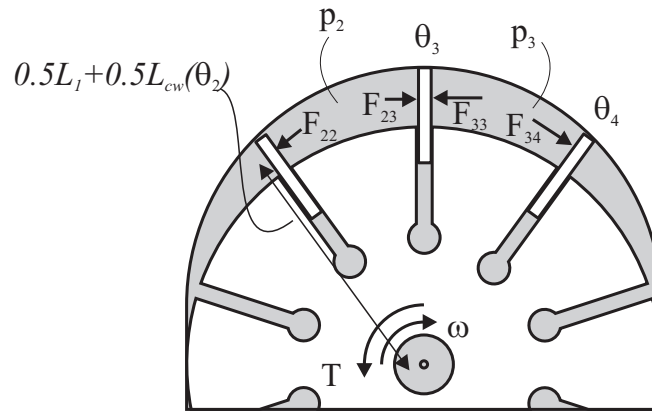


Figure 4.11: Forces on the vanes from the hydraulic seals

which can easily be derived from the geometry. From each vane a torque will act due to such a moment arm, and thus, summing over all active vanes gives the net torque of one of the pumping chambers of the vane pump

$$T = \frac{1}{2} \sum_{i=1}^{N/2} (L_1 + L_{cw}(\theta_i)) F_i \quad (4.62)$$

The two chambers of the pump are symmetrically aligned and if the pump is well-balanced, the two torque components from each chamber, will simply superimpose so that the total torque is twice the size of equation (4.62)

$$T = \sum_{i=1}^{N/2} (L_1 + L_{cw}(\theta_i)) F_i \quad (4.63)$$

Chapter 5

HiL and Real Time Adaptation

In order to simulate a real vehicle together with real hardware in the HiL environment, model response times have to be comparable to real response times. The ECU should see no difference. Given that the ECUs have fast and unknown signal reception times, the real time requirement leads to the demand that physical phenomena must be simulated as fast, or faster than they occur. To comply with these demands, the models developed in Chapter 4 may have to undergo changes that will reduce their accuracy. The goal with this chapter is to make such changes, but at the same time to ensure that these changes give the best possible accuracy.

5.1 Hardware-in-the-Loop

The HiL simulator used for simulation is made by dSPACE, and is depicted in Figure 5.1. To this system an ECU is connected in a loop like in Figure 1.1. The difference between a HiL system and a MiL system is that in HiL, the real ECU gets its input and produces its output over the same channel as it would in a real automotive system. Control signals from the ECU and simulated measured output signals will flow via LIN and CAN interfaces on real cables between the ECU and the simulator. It is also possible to connect other real hardware to the system. In MiL simulation, a model of the ECU software is used together with the simulated real world.

The dSPACE HiL simulator system contains software models of for example the engine, driveline and vehicle dynamics [24]. The models used in this simulator system have been developed by TESIS Dynaware. They are executable on a normal PC with MATLAB/SIMULINK, which makes MiL simulation available with a simplified ECU model to replace the actual hardware.



Figure 5.1: dSPACE HiL simulator [24]

In a first attempt to simulate the auxiliary devices, they are tested in such a MiL environment. In this first simulation environment, adaptations are made to the models to reach appropriate execution speed. Input and output considerations are also done at this time. Some of the needed input signals to the models developed in Chapter 4 can be found in the TESIS Dynaware engine model; control signals are sent from the hardware and have to be modelled. A well documented functionality to the ECU is a necessity in this stage. The Bosch units used for these simulations are all extensively documented.

5.2 Real Time Adaptation

For a diesel engine, a fairly high speed is usually about 3500 RPM. The pulley ratio differences will act as a gear and either heighten or lower this angular velocity to the rotating parts of the devices. The pulley ratios thereby limit the speeds of the models. As for the HiL simulator used in this work, it has a step time of 1.6 ms.

In this section some parameter values are introduced. For the system at hand they are either known from specifications or approximated typical values.

5.2.1 AC Compressor

Typically, the compressor pulley radius has 1.5 times the crankshaft pulley radius, limiting the compressor speed to 5250 RPM which equals 550 rad/s or 1.8 ms/rad. Internally, no variations of higher speed are modelled. The swash plate rotates with this speed, making the pistons oscillate with this frequency to complete a full compression and intake cycle in one period. With a simulation step-size of 1.6 ms, this process is possible to simulate with a reasonably good resolution (goes to a minimum at about 1.1 rad when engine speed reaches its maximum).

Simulating only the torque characteristics, without control loop back (i.e. with manual control, typically of the swash plate angle), requires no solution of differential equations, due to the steady state assumption. There is only one integration to find out the rotation angle. This makes the system automatically stable. When simulating the system with the fluid power controller described, some unstable behaviour are displayed. The system does not degenerate, but oscillates somewhat. Linearizing the model with the `linmod` command produces an A matrix that is close to singular and contains Not-a-Numbers. This could be a result of limits that is not possible to model correctly. For example, the pressure-relief valve is modelled simply as a saturation on the pressure inside the cylinder, the pressure calculations otherwise gives numbers approaching infinity as the volume is decreased. To determine stability of the model, the only option left is to test it in different situations and see if it diverges.

The simulator computation power and the compressor model complexity does comply, making it unnecessary to correct the simulator step-size due to computational power needs. This means that before simulating the model for a real development situation, one should test it with real parameters and investigate stability by trying to conjure an unstable situation.

5.2.2 Alternator

With a pulley ratio of 3, the alternator rotor speed typically goes up to 1100 rad/s. Typically, there are 12 poles on the alternator. Using equation (4.23), this corresponds to an electrical speed of 6600 rad/s. To model the in-cycle electrical behaviour with reasonable resolution (1 rad), a step time of 0.15 ms is required. Unfortunately, this does not comply with the simulator step time of 1.6 ms, about 11 times too slow for the wanted resolution. Electrical in-cycle behaviour will therefore not be possible to model. The fast alternating electrical variations are rather small compared to the average levels (see Section 6.1.2), but simulated at a reduced step-size, they can contribute to stability problems. Investigating the stability using the aforementioned MATLAB command `linmod` indeed exposes a number of poles in the right half

plane. Nevertheless, test simulations have not degenerated or oscillated much, and whether the stability problems lie in the presented alternator model, or in other connected models such as the battery model, cannot be said. Since functionality has been proven by tests, stability problems in the electricity system model are hereby noted and left.

However, the alternator has another component that causes problem with such low step-sizes. The PWM signal used to regulate the excitation current runs on a frequency of 400 Hz. With a simulation at approximately the same step frequency, the PWM will not be able to control the excitation current. The duty cycle will often only be able to take the values 0 or 1. Thus, the PWM signal loses some of its purpose. Some changes can be made to the model in order to achieve good results for the dynamic behaviour of the alternator.

One way is to simply have the PWM signal run on a lower frequency. This has the advantage of seeing the dynamics of the PWM signal in the control of the alternator, which can be good when developing control algorithms. Unfortunately, the variations from the PWM signal become larger than what they would become at a higher frequency. This is due to the inductance in the rotor circuit. An illustration of this can be seen in Figure 5.2. Along with the longer response time, there are also larger oscillations.

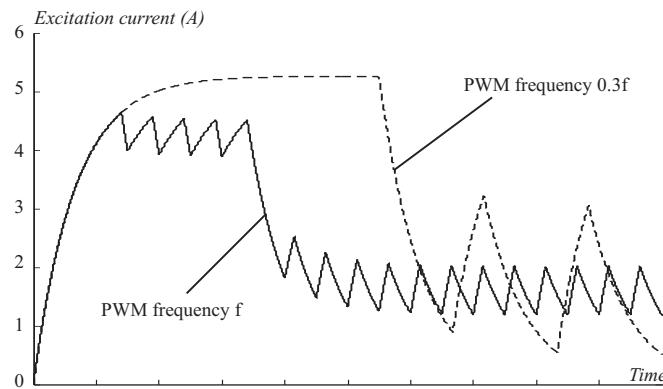


Figure 5.2: Illustration of simulated rotor current at a third of the actual PWM frequency (dotted), compared to the original PWM response.

A smaller change in frequency would result in smaller dynamic variations, and a PWM frequency of 300 Hz gives good enough resolution to simulate the system. In fact, seemingly good results are achieved even at the original 400 Hz frequency. This is due to the alternator speed, and the loads having slower dynamics than the PWM signal. The pulse width does normally not change between period to period. However, for a full-on functionality test a slight decrease in PWM frequency is recommended.

There are possibilities to run different parts of a system with different simulation step-times. In SIMULINK the block *rate transition* can be used for this purpose. In this work it has been used to give the battery model longer step-times during simulation. Battery quantities like state-of-charge (SOC) vary very slow, and it is therefore numerically profitable to simulate these dynamics at a lower step-time. This simulation step-time has to be an integer multiple of the whole system's step-time.

5.2.3 Power Steering Pump

An average model of the power steering pump, like the simple model presented in section 4.3.1 gives a constant torque. The more complex model take notice on in-cycle behaviour, but the average torque level remains the same. The simple model is therefore useable in a system where computational complexity is critical.

To model the in-cycle behaviour of the power steering pump, the simulation step-size matters. The in-cycle variations occur at a speed of N times that of the rotor speed, which in turn rotates with a speed proportional to the engine speed, depending on the pulley ratio. With $N = 10$ and a pulley ratio of 2, the in-cycle behaviour is not possible to model with the HiL system.

Chapter 6

Simulations and Validation

The simulations presented in this chapter have been run on a regular computer, or in the case of the HiL simulations, at one of dSPACE's simulation systems.

6.1 High Resolution MiL Simulations

In this section, MiL simulations mean simulations with constant or semi-constant (they can be manually changed during simulation) control signals. No ECU algorithms are used in this stage, and the simulations are fully done in SIMULINK. The simulation step-time is small enough to guarantee a good resolution.

6.1.1 AC Compressor

Parameters to this model are taken from several different sources, and some of them are simply estimated from what is reasonable for an automotive AC compressor. These "qualified guesses" are of course undesired and possible to improve by either direct measurements, reliable data sheets or by parameter estimation methods. Full knowledge of the control mechanism in the AC ECU was also missing during the course of this work. Much of this lack of information is grounds for more work, outside the scope of this thesis, something which is further treated in Chapter 8. For the simulations this means that they can only be seen as rough approximates.

A first simulation with a system where the control of the swash plate is manual shows good results. The simulation is done at 1800 RPM and gives a very reasonable torque as can be seen in Figure 6.1. The dynamics seen are from steps on the swash plate angle.

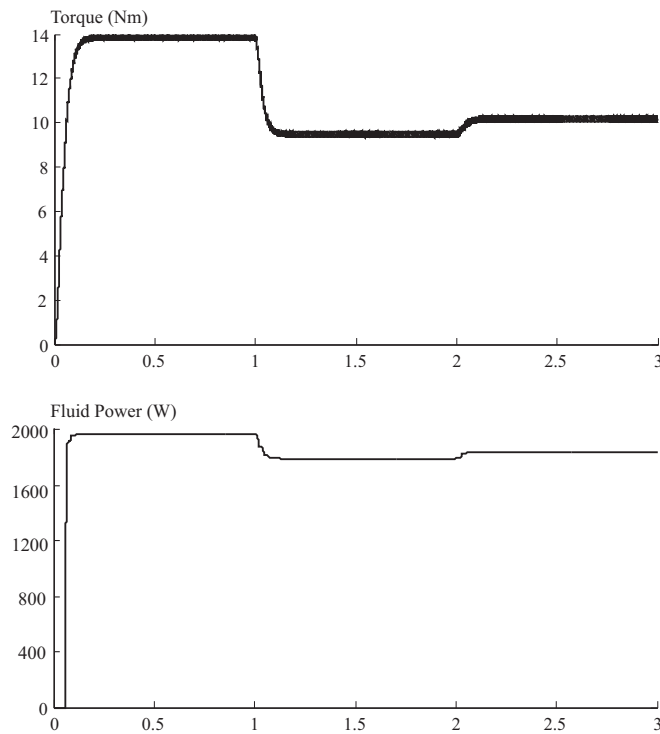


Figure 6.1: Dynamics of compressor torque and fluid power at changes in cooling capacity

There are small variations, which looks as noise, but a closer look reveals that these are torque fluctuations due to the phase difference of the individual piston movements. A compressor with fewer pistons would give a more uneven result, while one with more pistons would give a smoother curve.

6.1.2 Alternator

The parameters of this model are taken from several different sources, and results can therefore quantitatively differ slightly from the final desired simulation results. On the whole these simulations should however give good qualitative results.

The dynamics of the system are represented in Figure 6.2 where first a step is sent to the system in the form of an engine speed increase from 0 to 1000 RPM at time 0 and then a ramp, so that between times 3 and 6 the engine speed increases linearly to 2200 RPM.

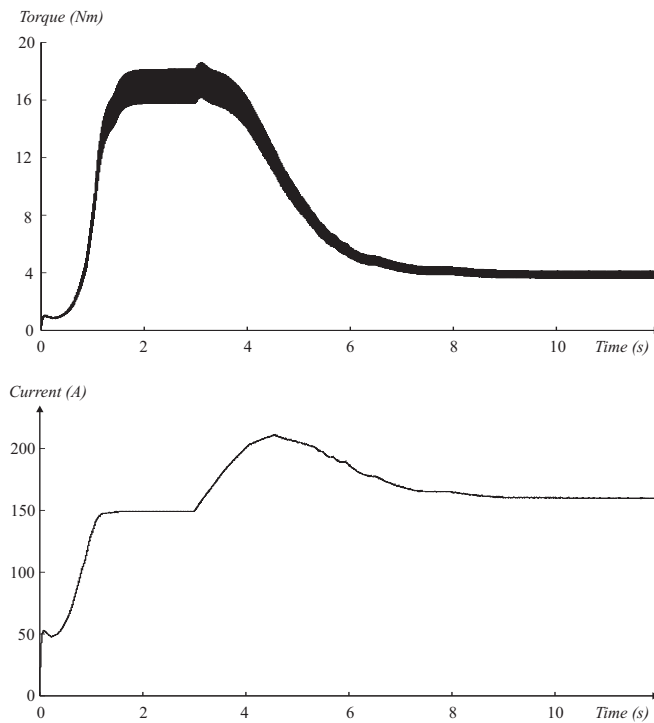


Figure 6.2: Dynamics of alternator torque and current at engine speed increases

This behaviour, where the torque is decreased at engine speed increase is expected. The current suffers at first from overshoot, but after a short period this error is leveled out.

More information about the model behaviour can be found in Figure 6.3. In this simulation plot the dynamics due to load changes are seen. The engine runs constantly at 1500 RPM. After 3 seconds the load needed is reduced from about 1800 W to 900 W. Such a large power drop does not normally occur, it roughly corresponds to a simultaneous shutdown of all the lamps, the electric back window heater and the electric power windows. The needed electricity is reduced, and thus the torque needed to produce the electricity is also reduced. After 7 seconds a load of 300 W (e.g. electric radiator) is turned on. The power need is heightened and the alternator takes more torque from the engine to produce this electricity.

The fast oscillations in the torque signal are due to the electric oscillations, and they have a periodicity exactly following the engine speed as

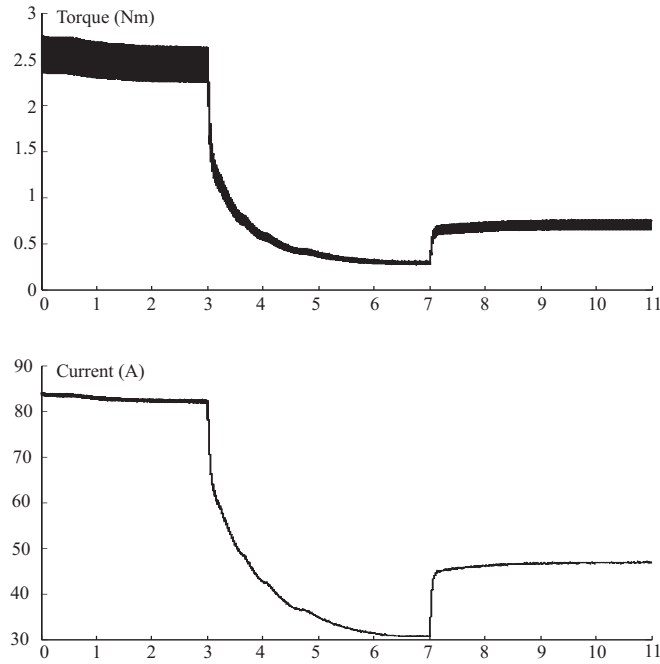


Figure 6.3: Dynamics of alternator torque and current at load changes

$$\omega_M = 6 \frac{P}{2} \omega_{eng} p_{ratio} \quad (6.1)$$

The number 6 in this equation comes from the rectifier bridge. Every single period of the electrical speed entering the bridge multiplies by 6 to the output, which is consistent with what Figure 2.10 illustrates. The reason for these not being dampened in the simulated torque is in much owing to the fact that the capacitor connected in parallel to the rectifier terminal is not modelled. Such a connection works as a simple low pass filter, thereby dampening the fast oscillations.

6.1.3 Power Steering Pump

Very few of the parameters used in this model are known for certain. The geometric quantities are estimated from pictures and the hydraulic properties like p_l and p_r are also typical values in hydraulics.

The in-cycle behaviour of the power steering pump is illustrated in Figure 6.4, together with the static torque (dotted) calculated from equation (4.39).

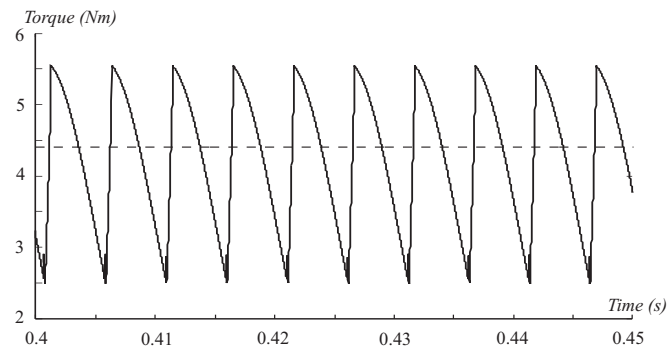


Figure 6.4: Power steering pump torque

6.2 HiL Simulation

The alternator model has been tested in the dSPACE simulator environment with a real ECU and a full engine model. The HiL environment comes with the CONTROL DESK interface which makes it possible to change parameters and control signals in real time. It is also possible to watch virtually any variable in the entire engine. An image of this interface can be seen in Figure 6.5.

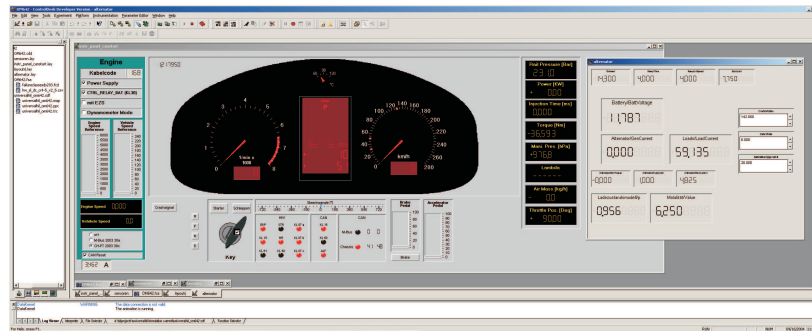


Figure 6.5: The CONTROL DESK interface

The simulation results are similar to those presented in section 6.1.2. When increasing the engine speed, with a fixed electric load, the torque taken by the device is lowered. The controller of the alternator regulates the torque after how much is needed to provide electric power to the different loads. The model responds properly to real time changes in load and to the control signals from the ECU. The ECU also responds to the model output.

6.3 Validity Discussion

To validate the models it is necessary to compare the real system with the simulated. Since the models are intended to simulate the vehicle against the engine ECU, the best validation would use the same ECU in the HiL setup and in the vehicle, as well as engine model parameters corresponding to vehicle parameters. Unfortunately no such measurements have been available in this work.

Instead, the available information must be used. Alternator measurements from another vehicle (with a different ECU and different engine and alternator parameters) have been done for different loads and different speeds, all of these are mean cycle values and give little information about the dynamic behaviour of the device. Comparing the torque at various speeds, some differences are visible, mainly in the speed-to-torque characteristics at high speeds and constant loads, these could be due to parameter differences or model errors. Some suggestions to how the model can be improved can be found in Chapter 8.

For the AC compressor, the only data available are approximate values of the maximum torque, usually about 20 Nm. With the approximated parameter values in the model, the torque stays below this level.

The power steering pump is constantly pumping and the torque variations are on average very small. In the simple model presented in this work, it is simply modelled as a constant. The complex model looks at the in-cycle behaviour which reveals that these variations can be substantial. Using a more complex model, which takes into account flywheel effects due to the rotor and pulley inertias is bound to smooth these variations. A discussion about how such a model can be constructed is done in Chapter 8. Of the three devices, the power steering pump takes the least amount of torque, and it is also the device with the least amount of control from different ECUs. The only control signal is on the relief valve which feeds back high-pressurized oil to the reservoir. This feedback does not effect the torque.

Another way to validate the models are to investigate them from an energy point of view. It is easy to see that the compressor and the alternator follows reasonable energy transfer principles. When more cooling power is needed in the vehicle, this can be remedied by raising the refrigerant flowing through the system. This fluid power does not come for free, but requires torque. For a controlled system, increases can occur in the cooling need, and in the engine speed. The former should heighten the torque and the latter make it smaller. The compressor model does these things.

As for the alternator. It can receive increases in the electrical power needed,

which requires a higher torque, and it can also use an increase in engine speed to produce the same amount of electricity with the same amount of torque. The alternator model presented here does these things.

Chapter 7

Conclusions

The AC compressor model covers the basic mechanics of the system very well. The mechanics for calculating the torque have previously been validated in [16]. To calculate the refrigerant compression as an adiabatic process is also a very good model, as can be seen in Figure 4.3. The dynamics of the strictly physical system is possible to model by using the models developed in this work. What makes this model incomplete is the lack of a qualitative model of its control mechanisms. The AC ECU and how it controls the compressor is of vital importance when modelling this device. The attempts of modelling them here are mere guesses of how they control the system.

Of the three devices examined and modelled in this work, the alternator is by far the most thoroughly treated, and many interesting characteristics of the torque signal can be seen in simulations. Simulations gives a good approximation of the real torque signal as validation shows. It is comparably of the same size at various speeds and battery voltages, and acts like one would expect in dynamic situations. The interaction with the existing battery model is very good. This makes the alternator model very useful for the ECU function development it was meant for. Simulations can be made early in the development process, which can make development processes simpler, thereby saving costs; even making such a project possible. Moreover, the model can also be used separately for alternator controller development.

The power steering pump models can be used to calculate the average torque, but since the torque is not controllable from the ECU, it is not very useable for function development. The simple model, which basically calculates a constant torque, is good enough for this purpose. The complex model though, can be used for other purposes. Such a use could be in acoustic analysis. All of the models are useful for this purpose. The in-cycle dynamic behaviours of the models are very likely to cause vibrations. Vibrational frequencies could very easily be extracted from the simulated models or from the models

themselves.

Chapter 8

Further Work

This work looks at the dynamic behaviour of the auxiliary devices, but it does not look into their behaviour due to dynamics from the engine. The engine acceleration is at all times assumed to be small enough to be ignored. This steady state is assumed because of the lack of information about the $\dot{\omega}$ signal. This makes the torque effects due to moment of inertia difficult to simulate. A solution to this problem would be to have the models driven by the engine torque instead of the engine speed. A SIMULINK scheme in Figure 8.1 illustrates the model structure this would result in.

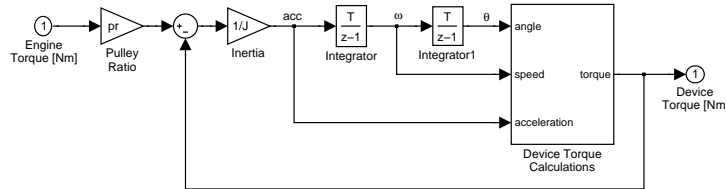


Figure 8.1: A suggested new model structure

This would of course make necessary some changes in the existing models, they would have to account for the acceleration of the engine, and thus to their own acceleration.

As chapter 7 says, the AC compressor control mechanism is not thoroughly modelled. A more detailed description of the AC ECU is necessary to build such a model. In a feedback control system like this it is important to know what sensors are used, and where they are situated. This work has modelled the flow through the system and used it to calculate the fluid power, which has been used as a control signal. This is only a qualified guess of how it really works. When the control system has been incorporated into the system, a full validation is necessary. To make that validation, a credible list of values on

parameters is necessary. Most of the compressor parameters are possible to simply measure as geometric distances, but for example the intake pressure and release pressure can be harder to measure and could probably be taken from product sheets from the manufacturer.

The alternator model has been validated by running it in a HiL simulation environment, and the dynamic behaviour of the model is as would be expected, however, it is not thoroughly validated. Such dynamic validations could be done to get a better estimation of the model's validity. Moreover, the static validation data could be of better quality. Suggested measurements of the alternator characteristics are the *open-circuit characteristic* (OCC) and the *short-circuit characteristic* (SCC), described in many books on electric machinery, for example [8, 11].

The power steering pump model is in need of both real parameters and a thorough validation. The validity of equation (4.58) should be tested by solving (4.57) for a number of different parameter sizes, including speeds.

References

- [1] Lars Nielsen and Lars Eriksson. *Course material Vehicular Systems*. Bokakademin, 1999.
- [2] Hariolf Gentner. *Vergleichende Untersuchung von mechanisch, elektrisch und thermisch angetriebenen Kälteanlagen zur Fahrzeugklimatisierung*. VDI-Verlag GmbH, Düsseldorf, Germany, 1995.
- [3] *Hydraulics Handbook*. Trade & Technical Press Limited, 8th edition, 1983.
- [4] CFC - Wikipedia, the free encyclopedia. Internet, 2004-05-02. <http://en.wikipedia.org/wiki/CFC>.
- [5] EU vill förbjuda dagens bilkyla. *Ny Teknik*, (43), 2004.
- [6] M.S. Bhatti. Enhancement of R-134a automotive air conditioning system. In *Int. Cong. & Expo.*, number 1999-01-0870, Detroit, Michigan, March 1999. Society of Automotive Engineers.
- [7] Michael A. Boles and Yunus A. Cengel. *Thermodynamics, An Engineering Approach*. McGraw-Hill, second edition edition, 1994.
- [8] A.E. Fitzgerald, Charles Jr. Kingsley, and Stephen D. Umans. *Electric Machinery*. McGraw-Hill, 5 edition, 1992.
- [9] David K. Cheng. *Field and Wave Electromagnetics*. Addison-Wesley, 2 edition, 1989.
- [10] Horst Bauer, editor. *Automotive electrics and electronics*. Robert Bosch GmbH, 3 edition, 1999.
- [11] Stephen J. Chapman. *Electric Machinery Fundamentals*. McGraw-Hill, 1999.
- [12] Ulrich Poestgens. *Servolenksysteme für Pkw und Nutzfahrzeuge*. Verlag Moderne Industrie, 2001.

-
- [13] Marcus Rösth. *Hydraulic Power Steering in Passenger Cars: Analysis, Modeling and New Functionality*. Lic thesis, Department of Mechanical Engineering, Linköpings Universitet, Linköping, Sweden, 2003.
- [14] Lennart Ljung and Torkel Glad. *Modellbygge och simulering*. Studentlitteratur, Lund, Sweden, 2 edition, 2004.
- [15] Dean C. Karnopp, Donald L. Margolis, and Ronald C. Rosenberg. *System Dynamics: Modeling and Simulation of Mechatronic Systems*. John Wiley & Sons, 3 edition, 2000.
- [16] N.D. Manring. The torque on the input shaft of an axial-piston swash-plate type hydrostatic pump. *ASME Journal of Dynamic Systems, Measurement, and Control*, 120:57–62, March 1998.
- [17] Du Pont technical information: Thermodynamic properties of HFC-134a. Internet. <http://www.dupont.com>.
- [18] Stefan Küppers. *Numerische Verfahren zur Berechnung und Auslegung von Drehstrom-Klauenpolgeneratoren*. Phd thesis 82, Fakultät für Elektrotechnik, Rheinisch-Westfälischen Technischen Hochschule Aachen, Aachen, Germany, January 1996.
- [19] Sheppard J. Salon. *Finite Element Analysis of Electrical Machines*. Kluwer Academic Publishers, 1995.
- [20] Vahe Caliskan. Modeling and simulation of a claw-pole alternator: Detailed and average models. Technical Report TR-00-009, Laboratory for Electromagnetic and Electronic Systems, Massachusetts Institute of Technology, October 2000.
- [21] C. Nordling and J. Österman. *Physics Handbook for Science and Engineering*. Studentlitteratur, 1996.
- [22] Mohieddine Jelali and Andreas Kroll. *Hydraulic Servo-systems: Modeling, Identification and Control*. Springer-Verlag, London, Great Britain, 2003.
- [23] J.F. Douglas, J.M. Gasiorek, and J.A. Swaffield. *Fluid Mechanics*. Longman Scientific & Technical, 3 edition, 1995.
- [24] dSPACE website, 2004-08-16. <http://www.dspace.de>.

Notation

Symbols

The following symbols and indexes are used throughout this text. The list is divided into four parts, one table for global symbols and one for symbols used in connection with each of the three devices.

F	Force	N
h	Simulation step-time	s
J	Moment of inertia	kg m ²
T	Torque	Nm
T_f	Torque from friction	Nm
ω	Angular velocity	rad/s
μ_f	Frictional constant	-
θ	Angle of the shaft	rad

AC Compressor

A_p	Area of a single piston	m ²
B	Compressor cylinder radius	m
C	Constant	m ² /s ²
m_p	Mass of a single piston	kg
N	Number of cylinders/pistons	-
p_i	Pressure in cylinder i	Pa
p_l	Intake pressure	Pa
p_r	Discharge pressure	Pa
r	Cylinder-to-shaft radius	m
R_i	Reaction force from piston i against the swash-plate	N
V	Specific volume	m ³ /kg
V_i	Instantaneous volume of piston i	m ³
V_G	Geometric displacement volume	m ³
x_i	Translational position of piston i	m
α	Swash plate tilt angle	rad
γ	Constant (spec. heat rel)	-
φ_i	Angle of piston i	rad

Alternator

The three armature windings, giving the three phases are denoted by indexes a , b and c . Index r implies the rotor. In this section, the angular quantities ω , θ are electrical, index m denotes their mechanical equivalents.

B	Magnetic flux density	T
i	Current	A
l	Stator length (at air gap)	m
\mathcal{L}_{ab}	Mutual inductance between winding a and b	H
L_{sr}	Stator-rotor mutual inductance	H
L_{ms}	Stator magnetizing inductance	H
P	Number of poles	-
r	Stator radius (at air gap)	m
R	Resistance	Ω
Φ	Magnetic flux	Wb
λ_a	Magnetic flux linkage of winding a	Wb
V	Voltage (EMF)	V

Power Steering Pump

A_b	Active area of intake or outlet port	m ²
b_l	Depth of the pumping chamber	m
C_d	Orifice discharge coefficient	-
L_1	Radius of rotor	m
L_2	Inner maximum radius of pump chamber	m
L_{cw}	Length from rotor centre to pump chamber wall	m
L_v	Length of vane	m
N	Number of vanes	-
p_b	Boundary pressure at orifices	Pa
p_l	Intake pressure	Pa
p_r	Discharge pressure	Pa
Q	Volumetric flow rate	m ³ /s
\mathcal{R}	Curve of vane centre of mass	-
V_{ij}	Hydraulic seal volume, between vane i and j , $j = i + 1$ (mod N)	m ³
V_p	Volumetric displacement	m ³
\dot{W}_{hyd}	Hydraulic power	W
\dot{W}_{mec}	Mechanical power	W
β	Hydraulic oil bulk modulus	Pa
Δ_N	Angle between two consecutive vanes, $2\pi/N$	rad
η	Efficiency parameter, $0 < \eta \leq 1$	-
$\phi_{1,2,3,4}$	Angles defining the inlet and outlets of pump	rad
ρ	Hydraulic oil density	kg/m ³
θ_i	Angle of vane i	rad

Abbreviations

The following abbreviations were used more or less frequently throughout the report.

AC	Air Condition/-ing
CAN	Control Area Network
CFC	Chlorofluorocarbon
ECU	Electronic Control Unit
EMF	Electromotive Force
HFC	Hydrofluorocarbon
HiL	Hardware-in-the-Loop
HPAS	Hydraulic Power Assisted Steering
KVL	Kirchoff's Voltage Law
LIN	Local Interconnect Network
MiL	Model-in-the-Loop
MMF	Magnetomotive Force
ODE	Ordinary Differential Equation
PWM	Pulse Width Modulation
R-134a	Refrigerant (1,1,1,2-tetrafluoroethane)
RPM	Revolutions Per Minute
SOC	State-Of-Charge
TDC	Top Dead Center

Copyright

Svenska

Detta dokument hålls tillgängligt på Internet - eller dess framtida ersättare - under en längre tid från publiceringsdatum under förutsättning att inga extra-ordinära omständigheter uppstår.

Tillgång till dokumentet innebär tillstånd för var och en att läsa, ladda ner, skriva ut enstaka kopior för enskilt bruk och att använda det oförändrat för ickekommersiell forskning och för undervisning. Överföring av upphovsrätten vid en senare tidpunkt kan inte upphäva detta tillstånd. All annan användning av dokumentet kräver upphovsmannens medgivande. För att garantera äktheten, säkerheten och tillgängligheten finns det lösningar av teknisk och administrativ art.

Upphovsmannens ideella rätt innefattar rätt att bli nämnd som upphovsman i den omfattning som god sed kräver vid användning av dokumentet på ovan beskrivna sätt samt skydd mot att dokumentet ändras eller presenteras i sådan form eller i sådant sammanhang som är kränkande för upphovsmannens litterära eller konstnärliga anseende eller egenart.

För ytterligare information om Linköping University Electronic Press se förlagets hemsida: <http://www.ep.liu.se/>

English

The publishers will keep this document online on the Internet - or its possible replacement - for a considerable time from the date of publication barring exceptional circumstances.

The online availability of the document implies a permanent permission for anyone to read, to download, to print out single copies for your own use and to use it unchanged for any non-commercial research and educational purpose. Subsequent transfers of copyright cannot revoke this permission. All other uses of the document are conditional on the consent of the copyright owner. The publisher has taken technical and administrative measures to assure authenticity, security and accessibility.

According to intellectual property law the author has the right to be mentioned when his/her work is accessed as described above and to be protected against infringement.

For additional information about the Linköping University Electronic Press and its procedures for publication and for assurance of document integrity, please refer to its WWW home page: <http://www.ep.liu.se/>